Evaluating the Effect of Grafting Ratio of Poly-L-Lysine-graft-Poly(ethylene) Glycol Co-polymers on the Esterolytic Activity of Encapsulated Enzymes

A thesis presented to the faculty of the Graduate School of Western Carolina University in partial fulfillment of the requirements for the degree of Master of Science in Chemistry

By Reginald Hines

Research Advisor: Dr. Rangika Hikkaduwa Koralege
Assistant Professor of Chemistry
Department of Chemistry and Physics

Committee Members: Dr. Channa De Silva and Dr. Maria Gainey
Western Carolina University, Cullowhee, NC 28723

Date: July 02nd, 2024

ACKNOWLEDGEMENTS

Firstly, I would like to thank and acknowledge my professor, Dr. Rangika Hikkaduwa Koralege, for her outstanding guidance during this project and my time at Western Carolina University. Her endless support has allowed me to push myself to become both a better chemist and individual. She has taught me so much in this short span of time with her boundless kindness and patience, I could not have received a better professor and I'm glad signing up for your p-chem I class which took me down this path.

I am extremely grateful to have Dr. Channa De Silva and Dr. Maria Gainey on my committee as their suggestions and advice has been undoubtedly helpful in completing this project. They have pointed out oversights that I missed or other avenues of research that haven't been considered. Without their expertise or constructive criticism this project would have been a shadow of its current state. I am thankful for Wes Bintz and Matt Burleson for their assistance in chemical supplies and instrumentation work, respectively. They have saved me numerous hours of work by their timely intervention.

I would also like to thank my friends and family for their support over the years of my academic journey. They have helped me see through to the end of this program and without them I would not be the person I am today nor be where I am currently. Despite the physical distance between us I know we are closer than ever.

Lastly, I would like to thank Western Carolina University and the Department of Chemistry and Physics. They have funded me through their 2023 and 2024 Summer Assistantships which has greatly helped the advancement of this project. I have met some of the greatest people that I know at Western Carolina University, and I am sure this place will continue to cultivate great individuals.

TABLE OF CONTENTS

LIST OF TABLES

LIST OF FIGURES

LIST OF ABBREVIATIONS

ATR-FTIR – Attenuated total reflectance Fourier transform infrared

BSA – Bovine Serum Albumin

DLS – Dynamic Light Scattering

d.nm – Diameter in nanometers

PBS – Phosphate buffered saline

PDI – Polydispersity index

PEG – Poly-ethylene glycol

PLL – Poly-L-lysine

PLL-g-PEG – Poly-L-lysine-graft-poly(ethylene) glycol

PNP- p-nitrophenol

mPEG-NHS – Methoxy poly-ethylene glycol N-hydroxysuccinimide

NP-PC- nanoparticle-protein corona

NMR – Nuclear magnetic resonance

NPs – Nanoparticles

STEM – Scanning transmission electron microscope

ABSTRACT

Nanoparticle therapeutics uses nano-scale particles to aid in the delivery of chemicals or biomolecular drugs such as therapeutic proteins, viral vectors, or anticancer medications. These nanoparticle drug delivery systems have many benefits such as (1) their large surface area to volume ratio, (2) stability, (3) increased solubility in aqueous solutions, and (4) protecting drugs or enzymes encapsulated from protease activity of the host. Protein drugs are an emerging class of therapeutics, and they offer many advantages such as higher specificity and potency than small molecule drugs. However, advancements in protein therapy are hindered by their poor stability, short *in-vivo* half life span, and immunogenicity. Encapsulation of therapeutic proteins within polymeric nanoparticles can protect them against detrimental environmental effects and protease activity, increase their solubility in aqueous solution, offer opportunities for controlled release, and increase their efficiency and stability. However, encapsulation may negatively affect the activity of an enzyme due to steric hindrance, restriction to diffusion-controlled access to the enzyme's active site, and conformational changes of the enzyme upon encapsulation.

The main goal of this project is to evaluate the effect of PEG grafting ratio of poly-L-lysine-graft-poly(ethylene) glycol (PLL-g-PEG) co-polymer on the catalytic activity of encapsulated enzymes. We synthesized 12 different co-polymers using differing molecular weights of PLL and varying amounts of PEG grafted (5%, 10%, and 15% by mass) onto PLL. The primary goals of this project include (1) synthesis of 12 different co-polymers and characterization using FTIR and NMR, (2) synthesis of protein-polymer nanoparticles by encapsulating a model protein, bovine serum albumin (BSA), (3) performing the physicochemical characterization including nanoparticle size and morphology using DLS and STEM respectively, (5) evaluating the encapsulation efficiency of BSA in each NP preparation, and (6) evaluating the esterolytic activity of the BSA in the nanoparticle complexes.

Our ATR-FTIR and NMR data confirmed the successful synthesis of the library of 12 different PLL-g-PEG co-polymers. The hydrodynamic diameter of the NP batches remained mostly consistent despite the increasing molecular weight of PLL or increase in PEGylation %. STEM particle sizes agreed well with the measurements taken by DLS, which ranged from 20 – 40 nm, and the NPs had a spherical morphology. The extent of BSA encapsulation in NPs was partial as evidenced by SDS-PAGE. Our major finding was that activity of the protein is not negatively affected upon encapsulation nor crosslinking since the esterolytic activity of BSA did not show a trend of decreasing. Interestingly, for some NP samples higher esterase-like activities were observed compared to non-encapsulated BSA which could be due to the accumulation of BSA proteins near the surfaces of these positively charged nanoparticle complexes.

CHAPTER I

INTRODUCTION

1.1—Nanotechnology and the importance of nanomaterials in drug delivery.

Nanotechnology is an emerging field that involves engineering nanoscale materials of varying chemical composition and shape. Nanomaterials exist on the nanoscale, and they're confined to around 1 – 1,000 nanometers (nm) in at least one dimension. Compared to their bulk counterpart these nanomaterials can be synthesized with superior magnetic, electrical, optical, mechanical, and catalytic properties using certain top down or bottom-up approaches [1]. Both inorganic and organic nanomaterials exist such as gold nanomaterials or dendrimers, likewise the shape of these nanomaterials can change from circular gold nanoparticles to cylindrical gold nanotubes. The ability to control and fine tune certain characteristics of these nanomaterials has made them an interesting material in the biomedical field as vehicles for disease diagnosis, drug delivery, biomedical imaging, and sensory techniques [2]. From a perspective focusing purely on drug delivery, nanotechnology can overcome several limitations of conventional delivery such as biodistribution in-vivo, target specific host cells/tissues, degradation of drug cargo, and the solubility of the encapsulated drug [3].

1.2—Protein therapeutics and their applications.

Protein therapeutics utilize biomolecules to treat difficult to cure diseases and they offer greater potency or specificity compared to small molecule drugs. There are multiple classifications of therapeutic proteins depending on their pharmacological activity (regulatory activity, cell specificity, protein vaccines, and protein diagnostics), the molecular composition of the protein (antibody-based drugs, blood factors, and hormones), or molecular mechanisms (binding non covalently to the target, affecting covalent bonds, or exerting activity without highly specific interactions like serum albumin) [4]. Every protein differs based on the amino acid sequence of each biomolecule which determines its three-

dimensional structure. Since the amino acid sequence of each protein varies from one biomolecule to another, based on the number and sequence of these amino acid groups, these proteins can have vastly different shapes from one another and often times the function of these proteins are inherently tied to the shape of it. These proteins while offering a plethora of advantages, such as replacing deficient and abnormal proteins or augmenting existing pathways within the body, have a few disadvantages associated with them like certain immunogenicity complications or short in-vivo lifespan [5]. There are other challenges present with proteins like their intrinsic susceptibility for aggregation, denaturation, or degradation via deamidation/oxidation in vitro or degradation by proteases in vivo [6]. Additionally, it's been observed that immunogenicity can be influenced by protein structure, composition, aggregation, and degradation [7].

1.3—Methods of protein encapsulation

To date many therapeutic proteins, viral vectors, and anticancer medication have been developed as nanocarrier complexes. There are different methods to prepare these nanocarriers, but they can be broken up into three broad categories: chemical methods, physical methods, and self-assembly processes like desolvation, electrostatic or hydrophobic interactions. Chemical methods consist of emulsion and complex coacervation while physical methods can be broken down into electro-spraying and nano-spray drying [8]. These methods involving nano scale delivery have advantages such as improved bioavailability, bioactivity, and controlled delivery over their bulkier counterparts. Polymeric nanoparticles are in an advanced stage of research in comparison to other materials [9]. Biodegradable polymers are a great interest as a drug delivery vehicle and poly(ethylene glycol) (PEG) is a commonly used polymer for its biocompatibility and 'stealth' properties [10]. Poly-lysine (PLL) is another polymer used for nanoparticle synthesis due to its cationic properties allowing for electrostatic self-assembly although it has been shown to have slight cytotoxic effects when used in higher cationic charge ratios, inducing nanoscale holes in the cell's membrane and overall reducing membrane permeability [11]. Therefore, it is vital to take all aspects of a polymer into consideration for nanoparticle synthesis. By

combining two polymers and finely controlling the nanoparticle shell's composition, we can aim to utilize both advantages they offer while minimizing their negative effects.

1.4—Potential adverse effects of encapsulating proteins

Although encapsulation can positively influence protein therapeutics by protecting the cargo from degradation, improving solubility of the drug, and even improving target specificity, it can inhibit the cargo in certain ways. PEGylation is a process in which PEG side chains are conjugated to a molecule and it offers stealth properties by creating a strong hydrophilic environment in which it helps trigger interactions in physiological environments. However, Michel *et al*. has reported that high amounts of PEGylation can negatively impact a protein's adsorption onto a nanoparticle complex resulting in potential conformational changes of the protein, restriction to the protein's active sites, or overall steric hinderance of the protein [12]. It's has been also reported that nanoparticles and proteins can form a nanoparticle-protein corona (NP-PC) in a biological medium, in which proteins that have a high affinity to the nanoparticle complex will bind on the surface or close to it, while proteins that have a low affinity to the complex will form a loose veil of protein interacting with other proteins or biomolecules around it [13]. Additionally, encapsulation within nanoparticles can potentially change the shape of these proteins due to steric hinderance, which risks changing the overall function of the protein, that could negatively affect the cargo's enzymatic activity. Due to the limitations of modern-day technology, understanding the molecular mechanisms of nanoparticle-protein binding more in depth could allow for the transition of nanoparticle drug delivery systems from scientific research to clinical trials more effectively.

1.5—Our approach to evaluate the effect of poly-L-lysine-graft-poly(ethylene) glycol (PLL-g-PEG) co-polymers on encapsulated proteins.

Our goal in this project is to synthesize twelve different PLL-g-PEG co-polymers to then synthesize twelve different batches of nanoparticles by encapsulating BSA. Four different molecular weights of PLL will be used and three different mass percentages of PEG will be grafted onto PLL to

create our PLL-g-PEG co-polymer library. Figures 1 and 2 show schematic diagrams of different variations present in our co-polymer library.

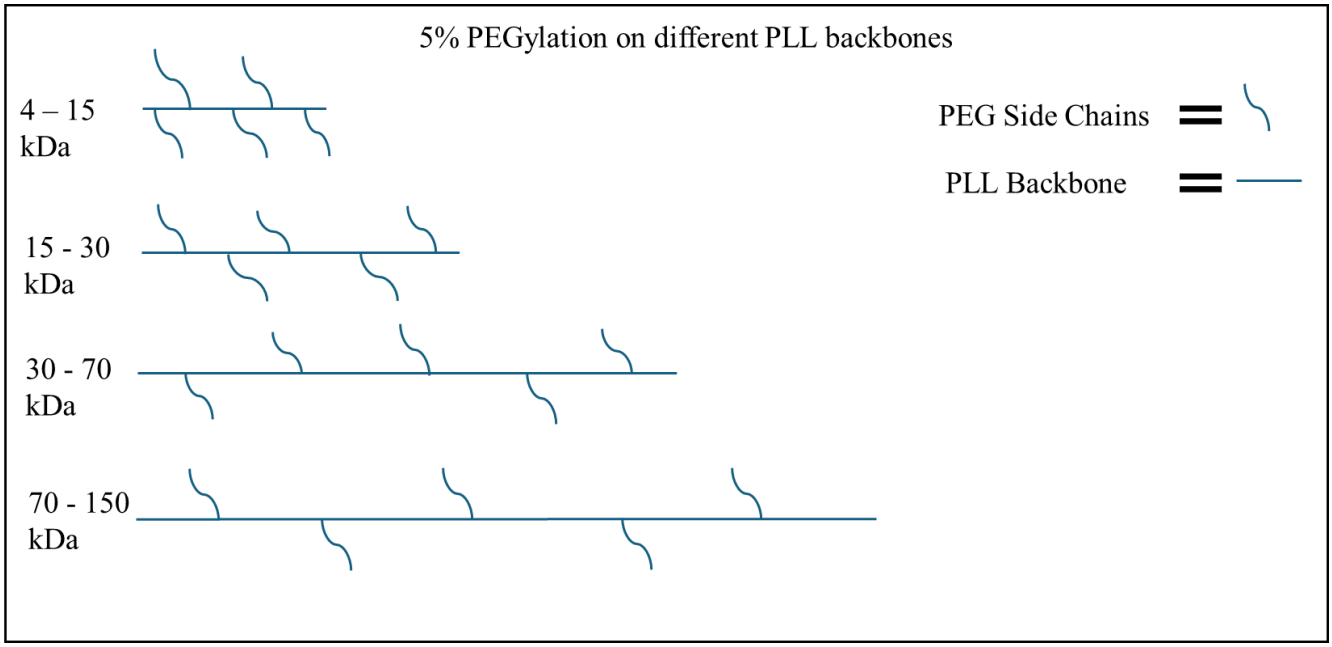

Figure 1: Schematic diagram showing 5% PEGylation on varying molecular weights of PLL backbone.

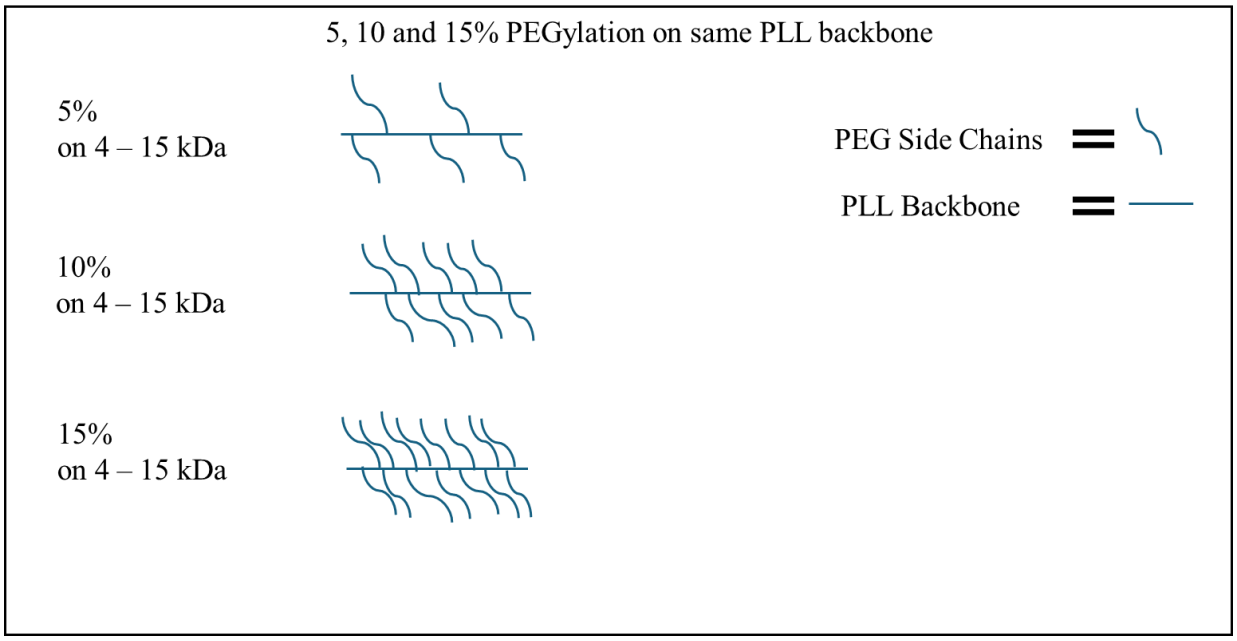

Figure 2: Schematic diagram showing 5, 10, and 15% PEGylation on the same molecular weight of PLL backbone.

Figures 3 and 4 show the chemical structure of our co-polymer, PLL-g-PEG and the chemical reaction between N-Hydroxysuccinimide (NHS) group of mPEG-NHS and primary amine groups of PLL to form the PEG grafted co-polymer, PLL-g-PEG.

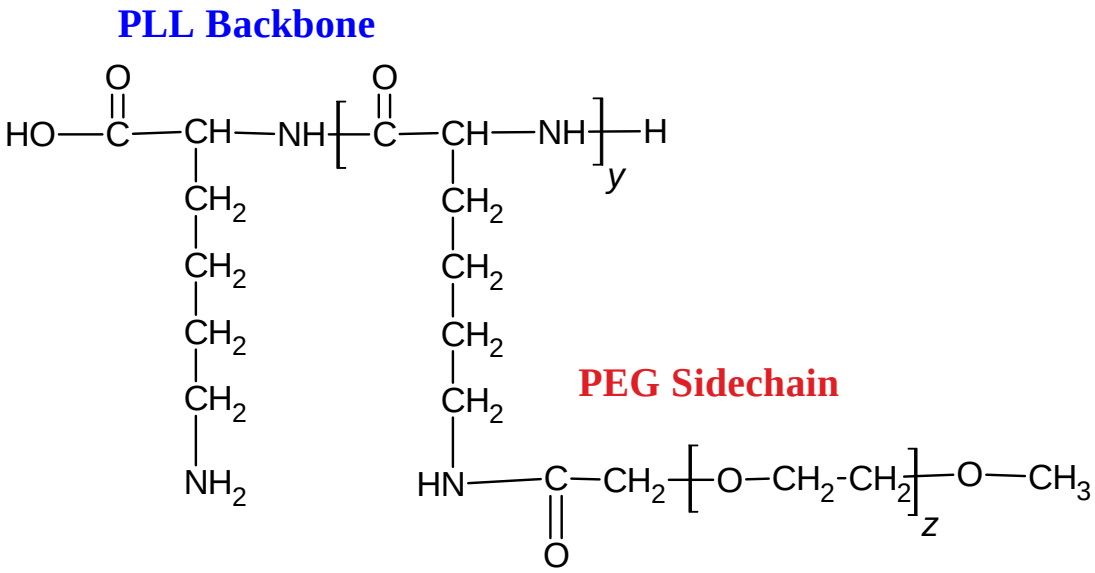

Figure 3: Chemical structure of PLL-g-PEG

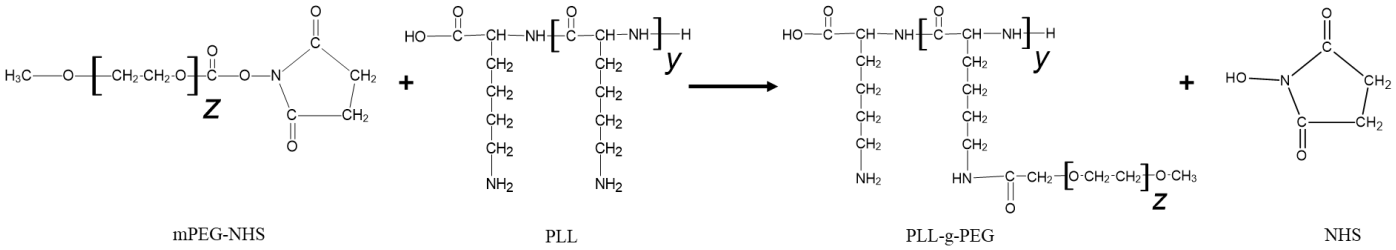

Figure 4: Chemical reaction between N-Hydroxysuccinimide (NHS) group of mPEG-NHS and primary amine groups of PLL to form the PEG grafted co-polymer, PLL-g-PEG.

We anticipate that our NP complexes may also have NP-PCs as described in the previous section since negatively charged BSA could have higher affinities to positively charged co-polymer surface on the NPs. Figure 5 shows a schematic diagram of possible BSA corona and/or adsorption on the NP surface apart from encapsulation. We hypothesize that higher percentages of PEGylation may inhibit BSA being adsorbed onto the surfaces of the nanoparticles due to steric hindrance while lower amounts of PEGylation will allow more BSA proteins to be adsorbed onto the cationic surface of the co-polymer, although lower amounts of PEGylation will negatively affect the nanoparticle's immunogenicity which is a concern with in-vivo experiments.

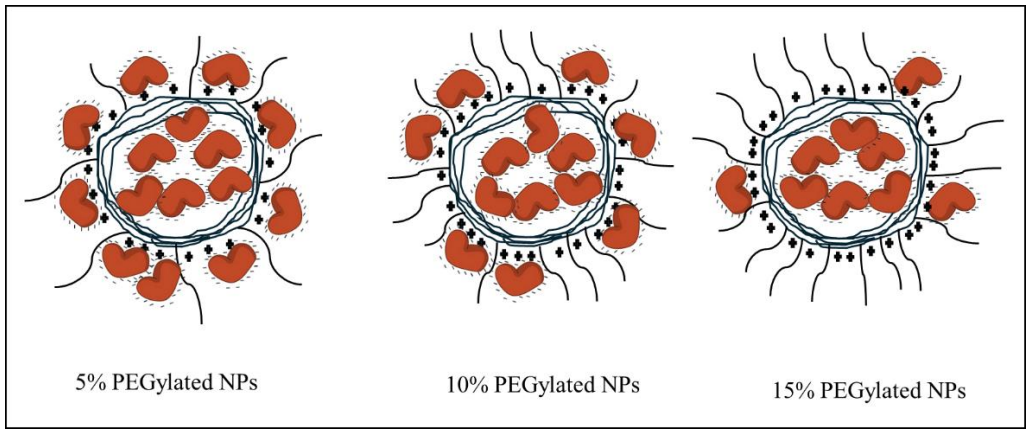

Figure 5. Schematic diagram of 5, 10, and 15% PEGylated nanoparticles.

The nanoparticle complexes are formed via electrostatic interactions between the cationic co-polymer, PLL-g-PEG and the negatively charged bovine serum albumin (BSA) at physiological pH of 7.4. Figure 6 shows a schematic diagram of nanoparticle assembly.

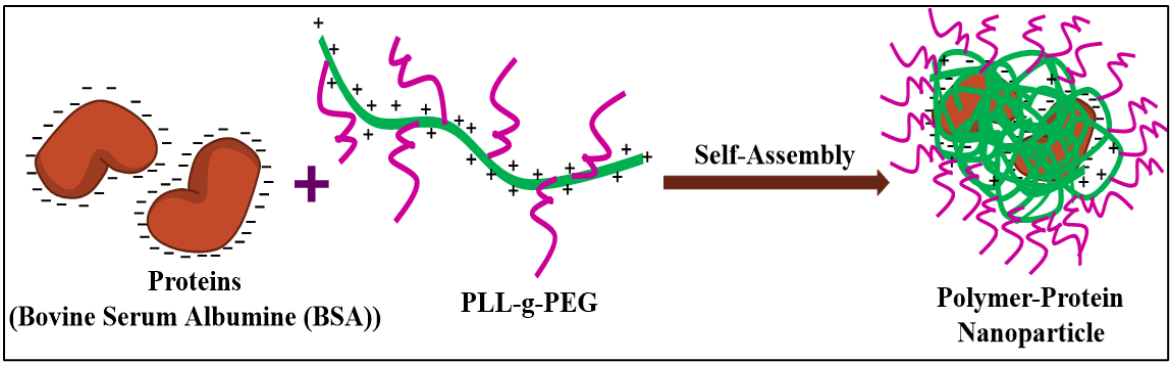

Figure 6. Electrostatic assembly of nanoparticles between positively charged PLL-g-PEG co-polymer and negatively charged BSA.

BSA is a commonly used model protein for its similarity to human serum albumin, the low cost of producing this animal protein, and it has several different methods of detection. Serum albumin is a protein tied to the health of its host organism due to its role of maintaining plasma pressure and acting as a transporter for biomolecules in vivo, with BSA being an important indicator of bovine health [14]. The charge of BSA depends on the pH conditions of the solvent. With an acidic environment lower than its isoelectric point (~5 pH), BSA is positively charged due to protonation of amine groups and in a basic environment higher than its isoelectric point, it is negatively charged due to deprotonation of carboxyl moieties [15]. Following the nanoparticle synthesis as shown above in Figure 5, the NP complexes will be crosslinked with glutaraldehyde. Crosslinking with glutaraldehyde helps retain the encapsulated proteins within NPs and it will also affect the porosity of the polymer matrix [16]. The chemical structure of glutaraldehyde and the chemical mechanism of glutaraldehyde crosslinking reaction are shown in Figures 7 and 8. Crosslinking reaction occurs between free primary amine groups of the co-polymer and the two carbonyl groups on the glutaraldehyde, forming what's commonly known as a 'Schiff' base [17,18].

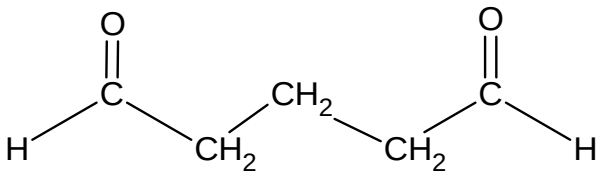

Figure 7. Chemical structure of glutaraldehyde.

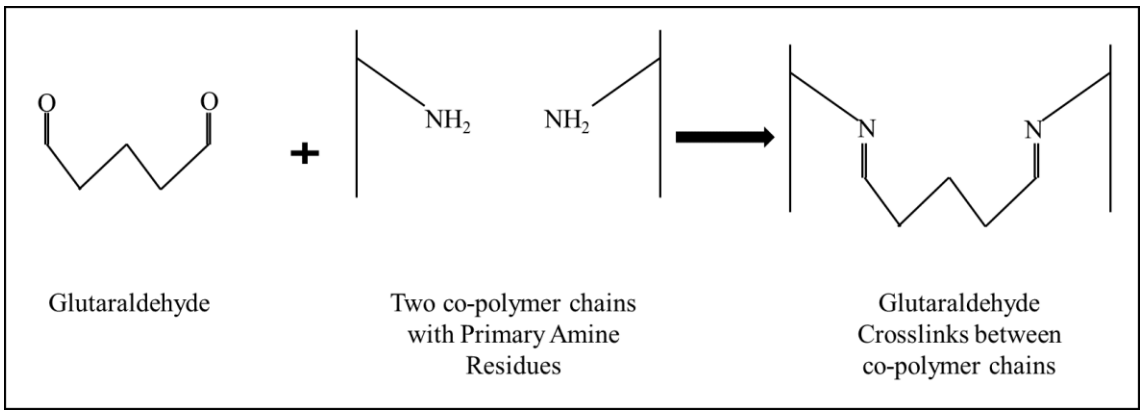

Figure 8. The formation of glutaraldehyde crosslinks between primary amine groups of adjacent co-polymer chains forming a 'schiff' base.

CHAPTER II

EXPERIMENTAL METHODS

2.1—Materials

Poly-L-lysine•HBr with molecular weights of 4 – 15, 15 – 30, 30 – 70, and 70 – 150 kDa, p-nitrophenyl caprylate, and isopropyl alcohol were purchased from Sigma-Aldrich. Methoxy-PEG succinimidyl carboxymethyl ester (mPEG-NHS) with a molecular weight of 5 kDa was purchased from Creative PEGWorks. Bovine serum albumin, Glutaraldehyde (50%), acrylamide/bisacrylamide (37.5:1) and other polyacrylamide gel casting and running materials were purchased from Fisher Scientific. The reagents were used without further purification. Isopropanol and 4-nitrophenyl octanoate were purchased from Alfa Aesar for the activity assay. The phosphotungstic acid for STEM was purchased from Electron Microscopy Science.

Phosphate buffered saline was -prepared using sodium chloride purchased from Sigma-Aldrich, potassium chloride obtained from Carolina Biological Supply, disodium phosphate from the Sigma Chemical Company, and monopotassium phosphate bought from Reagents Inc. All the reagents were dissolved in 800 mL of distilled water and adjusted the pH to 7.4 using a vernier pH sensor before bringing the total volume to 1 L with distilled water.

2.2—PLL-g-PEG co-polymer synthesis

Primary amine groups of the PLL backbone were modified with the succinimidyl ester group on the mPEG-NHS to produce PLL-g-PEG. To prepare the PLL-g-PEG co-polymer library, 15 mg of PLL•HBr from each molecular weight was dissolved in 400 µL of phosphate buffered saline (PBS, pH 7.4) and varying amounts of 5 kDa mPEG-NHS were added to the dissolved PLL. (Table 1 summarizes different grafting ratios (by weight) and the amount of mPEG-NHS added to prepare the 12-co-polymer

library). The PLL-g-PEG mixture was allowed to react for 1 hour before being washed three times with 50/50 (v/v) mixture of PBS and ethanol, and a final wash of pure ethanol in a 10 kDa and 100 kDa centrifugal concentrator, depending on the molecular weight of the PLL used in the synthesis. After the washes, the co-polymers were dried using a rotary evaporator before being used or stored at -20°C. A schematic diagram of the co-polymer formation is depicted in Figure 9.

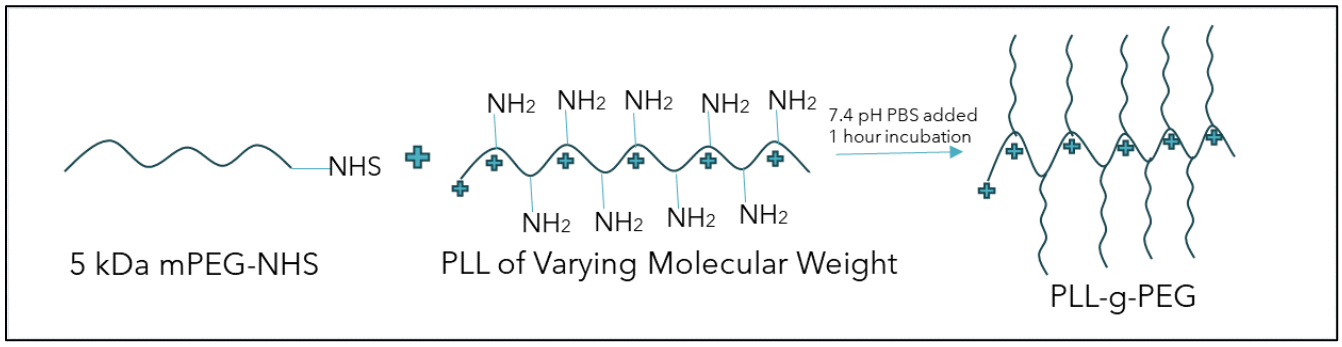

Figure 9. A schematic diagram of the co-polymer formation.

Table 1. Amounts of mPEG-NHS used to synthesize the co-polymer library of PLL-g-PEG.

PLL Molecular Weight (kDa)	Amount of mPEG-NHS, 5 kDa/ mg		
	5% Grafting Ratio	10% Grafting Ratio	15% Grafting Ratio
4 – 15	29.259	58.517	87.776
15 – 30	29.275	58.550	87.825
30 – 70	29.259	58.500	87.750
70 – 150	29.258	58.500	87.775

2.3—Synthesis of bovine serum albumin (BSA) encapsulated nanoparticles

A BSA stock solution of 1 mg/mL was prepared by dissolving 1.0200±0.0001 mg of BSA protein in 1.00 mL of PBS. BSA was encapsulated using 12 different PLL-g-PEG co-polymers, with a co-polymer: protein mass ratio of 7:1. The stock BSA solution was dissolved in PBS to a concentration of 0.266 mg/mL and PLL-g-PEG co-polymer was dissolved in PBS at a concentration of 6 mg/mL. The co-polymer (7.5 uL) was then added to the BSA solution (25 uL) dropwise, while gently vortexing, followed by incubation of the mixture for 1 hour at room temperature. To stabilize the polyion complexes formed in this study, the free primary amine groups left in the polymer chains of the NPs were cross-linked with 5 uL of glutaraldehyde solution (0.025% in PBS) and incubated for another 3 hours at room temperature. The electrostatic assembly of NPs and the glutaraldehyde crosslink formation were depicted in Figures 6 and 8, respectively, in the introduction chapter. The final BSA concentration in NPs was 0.177 mg/mL.

2.4—^{1}H-NMR Analysis of PLL-g-PEG polymers

PLL-g-PEG copolymers (5.0800±0.0001 mg) were dissolved in 750 uL of deuterated chloroform ($CDCl_3$) solvent and analyzed using Bruker 400 MHz NMR with a 5-mm tunable probe for ^{1}H NMR. This was done to confirm the grafting of PEG onto PLL using ^{1}H-NMR spectroscopy. Although PLL is not very soluble in $CDCl_3$ it helped to get rid of the prominent water peak shown around 3.3 ppm.

2.5—Attenuated Total Reflectance Fourier Transformed Infrared Spectroscopy (ATR-FTIR) analysis of PLL-g-PEG polymers

ATR-FTIR was performed on the 12 PLL-g-PEG co-polymers synthesized to confirm their properties. A few milligrams of each co-polymer, PLL, and mPEG-NHS, were analyzed using a Thermo iS10 FT-IR Centarus Microscope with 128 scans performed at a resolution of 8.

2.6—Dynamic Light Scattering (DLS) of BSA nanoparticles

The size distribution of 0.177 mg/mL BSA NPs (100 μL) was determined using DLSwith a Malvern Zetasizer ZS Particle Size Analyzer equipped utilizing a 4 mW 632.8 nm laser. All the measurements were done at 25 °C and using a Brand Tech Scientific ZEN0040 40 μL Ultra-Micro disposable cuvette with a stopper.

2.7—Scanning-Transmission Electron Microscopy (STEM) of BSA nanoparticles

The morphology and size of the NPs were analyzed by STEM. NP samples (10 μL), with a concentration of 0.177 BSA, were deposited onto Lacey/Formvar Carbon 200 mesh, copper grids using a drop-casting method and allowed to air-dry at room temperature for overnight. The samples were then negatively stained with 10 μL of phosphotungstic acid (pH 7.4) for one minute and the excess stain was wicked off the grid using filter paper. The samples were allowed to dry for two hours before observation using a Thermo Fisher Apreo 2 SEM equipped with a TEM detector.

2.8—Gel retardation assay

The extent of BSA encapsulation of NPs was determined by a gel retardation assay. SDS-PAGE gels (12%) were hand casted and loaded with either NP samples or a control of non-encapsulated BSA protein. NPs were run at 200 V under non-reducing conditions using a BIO RAD Mini-PROTEAN® Tetra Cell apparatus until the dye front reached the bottom of the gel. The SDS-PAGE gels were stained with Coomassie G-250 then destained before imaging.

2.9—Measurement of retention of protein catalytic activity

To evaluate the effect of encapsulation on protein function, the esterase activity of encapsulated BSA toward p-nitrophenyl caprylate was determined using a method reported by Córdova *et al*. [19]. The ester hydrolysis of encapsulated BSA was measured by monitoring the release of p-nitrophenol spectrophotometrically. To measure the esterolytic activity, 5 μL of 6 mM p-nitrophenyl caprylate in isopropanol was added to 100 μL of NPs, with a concentration of 0.177 BSA, and the controls (Free BSA at 0.177 mg/ml and BSA Free NPs). Three different controls were used including, free BSA, BSA free nanoparticles, and PBS. The mixture was allowed to incubate for 20 hours at 37°C before absorbance measurements were taken at 410 nm on a SpectraMax iD5 multimode plate reader.

CHAPTER III

RESULTS & DISCUSSION

3.1-PLL-g-PEG co-polymer library

In this project, we focused on determining how different PEGylation percentages (5, 10, and 15%) onto PLL backbone with different sizes (4-15, 15-30, 30-70, and 70-150 kDa) could affect the enzymatic activity of an encapsulated enzymes within NPs. Enzymatic activity of the therapeutic enzyme could be reduced due to steric hindrance, diffusion-controlled access to the enzyme's active site, and conformational changes of the enzyme upon encapsulation. Previous research has shown that variations in co-polymer architecture influence the encapsulation and stability of a protein. Therefore, these variations will also influence the activity of the enzymes. [20]

The hypothesis behind the synthesis of this PLL-g-PEG co-polymer library was to change the architecture of each co-polymer and thereby change the NP structure. As you increase the size of the PLL backbone keeping the PEGylation percentage to be the same, the distance between PEG side chains will increase as depicted in Figure 1 in the introduction section. Increasing the PEGylation percentage on a given PLL backbone will increase the number of PEG side chains and decrease the distance between them as depicted in Figure 2 in the introduction section. This will result NPs with different porosities and hence different properties.

3.2-Synthesis of BSA encapsulated PLL-g-PEG nanoparticles

The synthesis of the BSA encapsulated NPs was performed using BSA at an initial concentration of 0.266 mg/mL been added to a PLL-g-PEG solution at a concentration of 6 mg/mL. The final encapsulated BSA in the NP complexes was estimated to be at 0.177 mg/mL according to the dilution

steps along the synthesis procedure. However, it is impossible to calculate the concentration exactly unless lysis of the NP complexes is performed.

The uptake of BSA into the NP complex depends on encapsulation of the cargo inside and the adsorption of the negatively charged cargo onto the exterior surfaces of these NP complexes. Apart from encapsulation, we hypothesized that the NP complexes with a lower PEGylation percentage may have a higher adsorption of these BSA proteins onto the surfaces due to positively charged surface being more readily exposed or available.

3.3-Characterization of PLL-g-PEG using ATR-FTIR spectroscopy

During the co-polymer formation, the N-hydroxysuccinimide (NHS) group present in the mPEG-NHS reacts with the primary amine groups present in PLL (shown in Figure 4 in the introduction chapter) at physiological to slightly alkaline conditions (pH 7.2 to 9) to yield stable amide bonds resulting in PLL-g-PEG co-polymer formation and releases NHS. Figures 10-13 show the FTIR spectra of all the co-polymers.

ATR-FTIR spectroscopy was used to confirm the presence of functional groups present in each polymer and the attachment on PEG onto PLL. Due to its hygroscopic nature PLL has a broad band around 3000-3200 cm^{-1} region. PLL has a primary amine group that shows around 3270 cm^{-1} and 3200 cm^{-1} for N-H stretching which depends on the configuration and protonation of -NH_2 group [21]. All the co-polymers or polymers have this band except PEG which distinctly lacks an amine group. The -C-H stretching of PEG has a prominent peak around 2868 cm^{-1} and another peak associated with the -C=O ester functional group's stretching [22]. The -NH-C=O group around 1690 cm^{-1} resulted from successful grafting of PEG onto PLL to produce PLL-g-PEG which confirms the co-polymer formation and this resulted in a shift of wavenumber compared to the -C=O functional group present in PEG around 1700 cm^{-1}.

Table 2. FTIR stretching of PLL-g-PEG functional groups.

Functional Group	Wavenumber (cm^{-1})
-NH_2- of PLL	3200 - 3270
-NH-C=O of PLL-g-PEG	1690
-CH- of PEG	2868
-C=O of PEG	1700

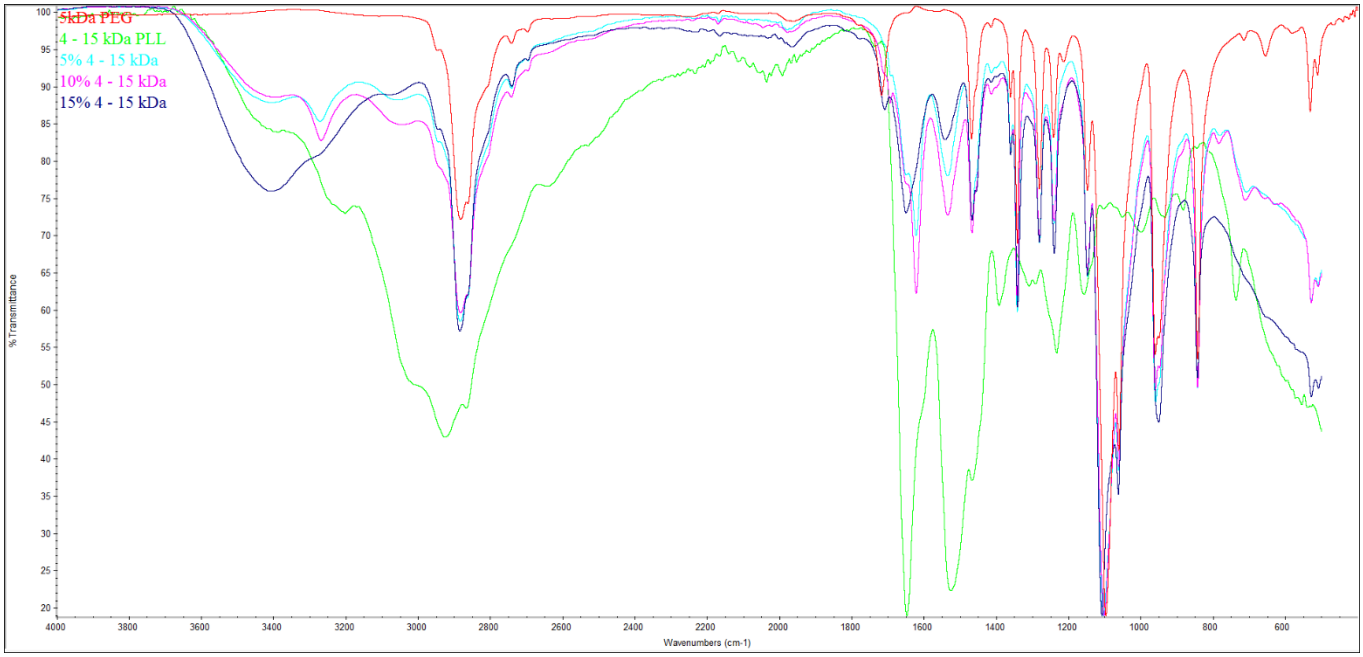

Figure 10. FTIR spectra of co-polymers resulted from 5, 10, and 15% PEGylation onto 4 – 15 kDa PLL.

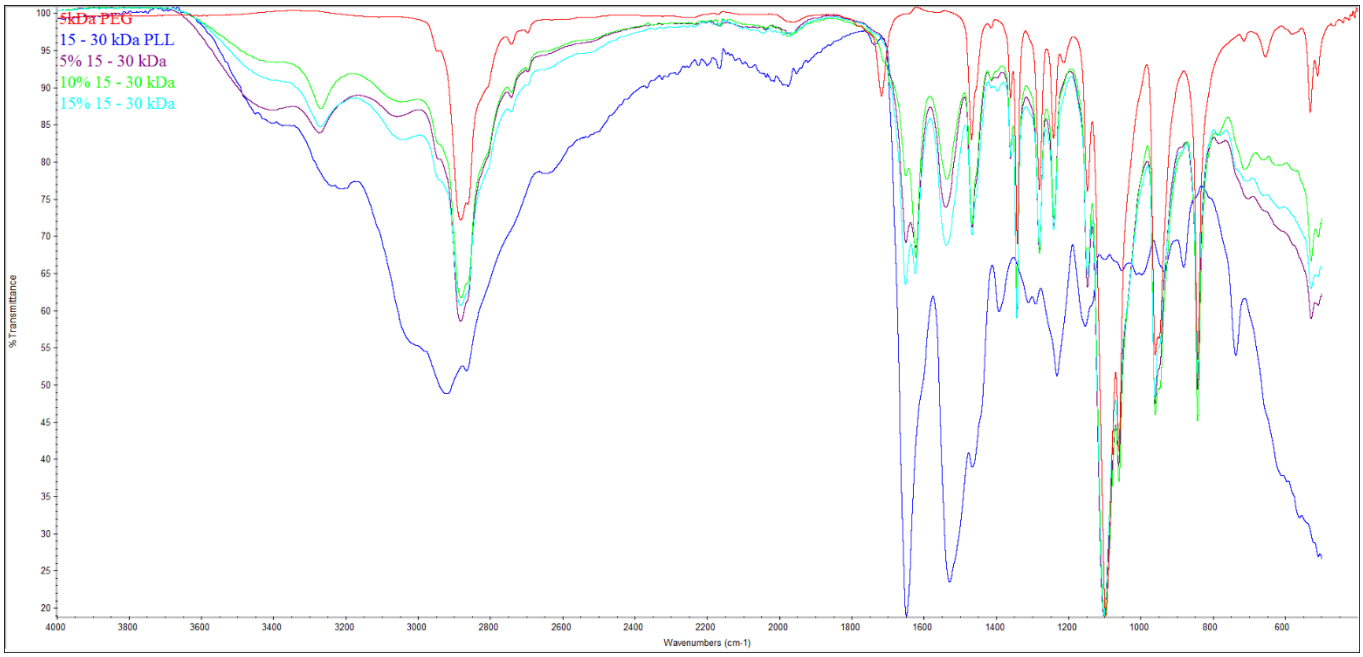

Figure 11. FTIR spectra of co-polymers resulted from 5, 10, and 15% PEGylation onto 15 – 30 kDa PLL.

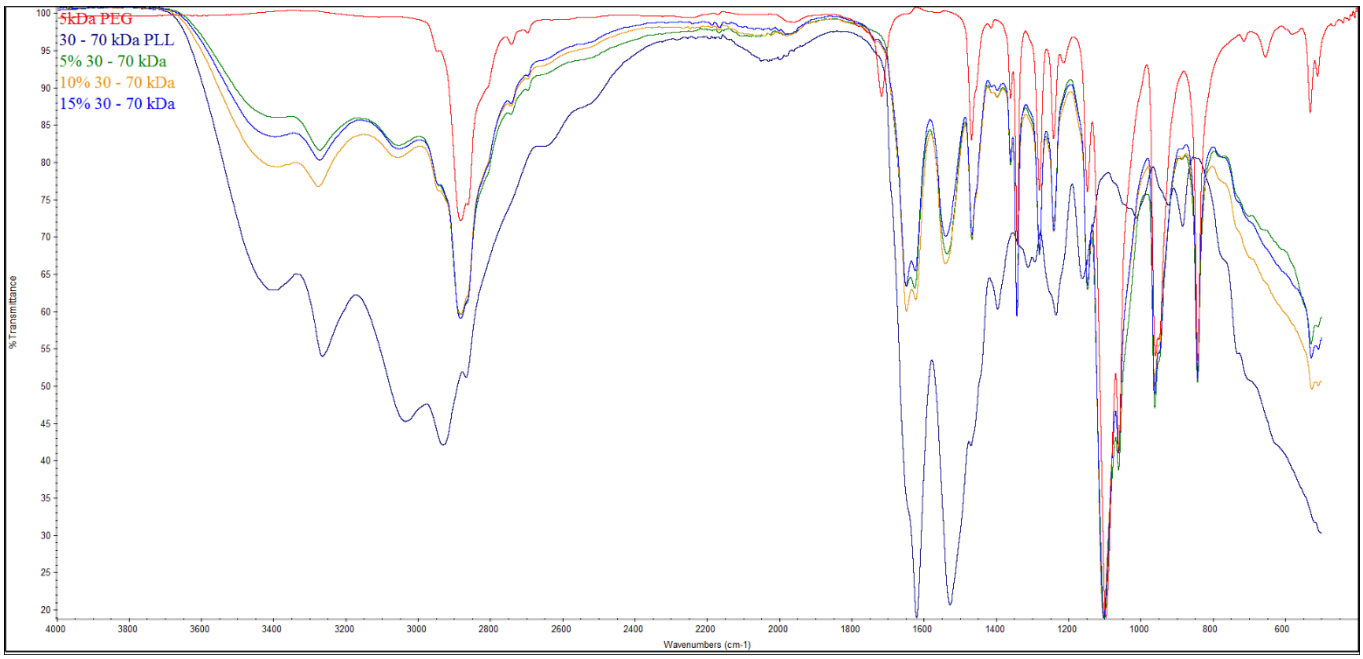

Figure 12. FTIR spectra of co-polymers resulted from 5, 10, and 15% PEGylation onto 30 – 70 kDa PLL.

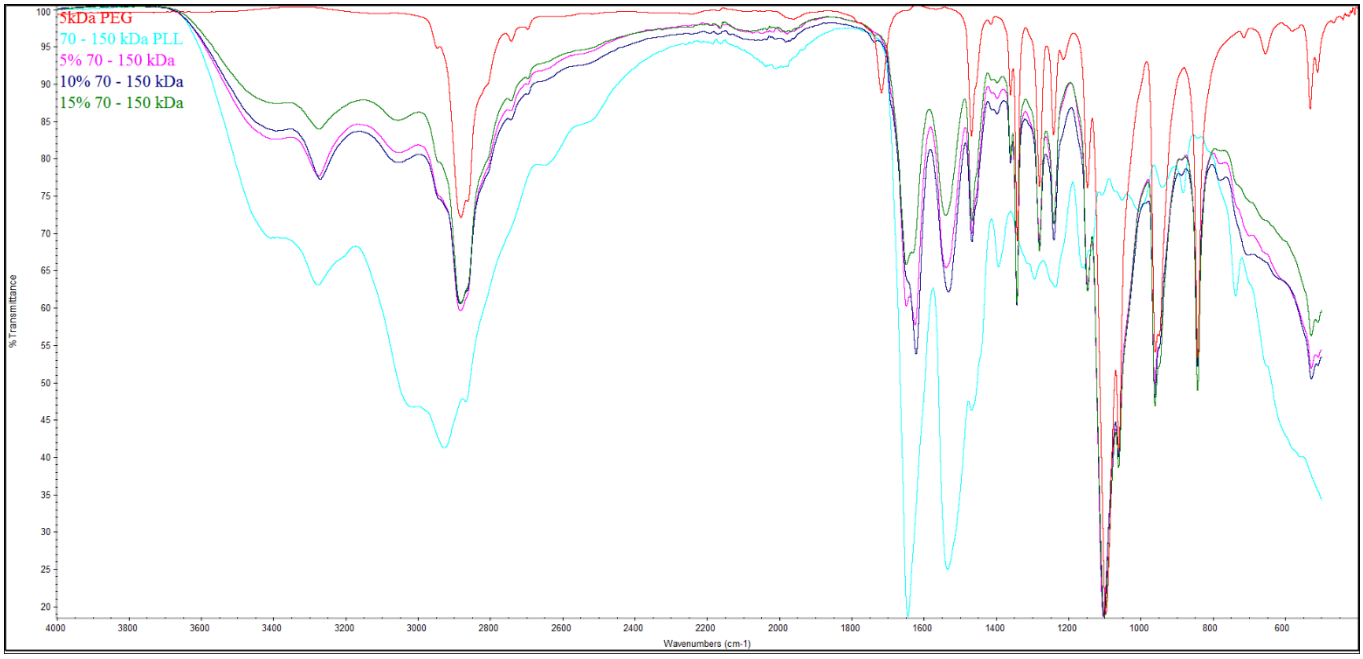

Figure 13. FT-IR spectra of co-polymers resulted from 5, 10, and 15% PEGylation onto 70 – 150 kDa PLL.

3.4- Characterization of PLL-g-PEG co-polymer using ^{1}H NMR

The PLL-g-PEG co-polymers were characterized using ^{1}H NMR spectroscopy to confirm the formation of the co-polymer. Table 3 summarizes the chemical shifts observed for each functional group. The chemical structures of PLL-g-PEG, PLL, and mPEG-NHS are shown in Figures 3 and 4 in the introduction chapter. Figures 14 - 25 have prominent peaks associated with -CH_2CH_2O- functional group at 3.7 ppm and -OCH_3 functional group at 3.3-3.4 ppm for PEG side chains [23]. The -CH- functional group is associated with PLL and is found around 4.1 – 4.3 ppm. The -$CH_2CH_2CH_2CH_2$- functional groups of the PLL are shown at 1-2 ppm. The PEG functional groups shown at 3.7 ppm and 3.3-3.4 ppm confirms that PEG was successfully grafted onto PLL.

Table 3. Chemical shifts associated with different protons of PLL and PEG.

Functional Group	Chemical Shift (ppm)
- CH_2 groups on PLL	1-2 ppm
-CH_2CH_2O- of PEG	3.7 ppm
-OCH_3 of PEG	3.3-3.4 ppm
-CH- of PLL	4.1-4.3 ppm

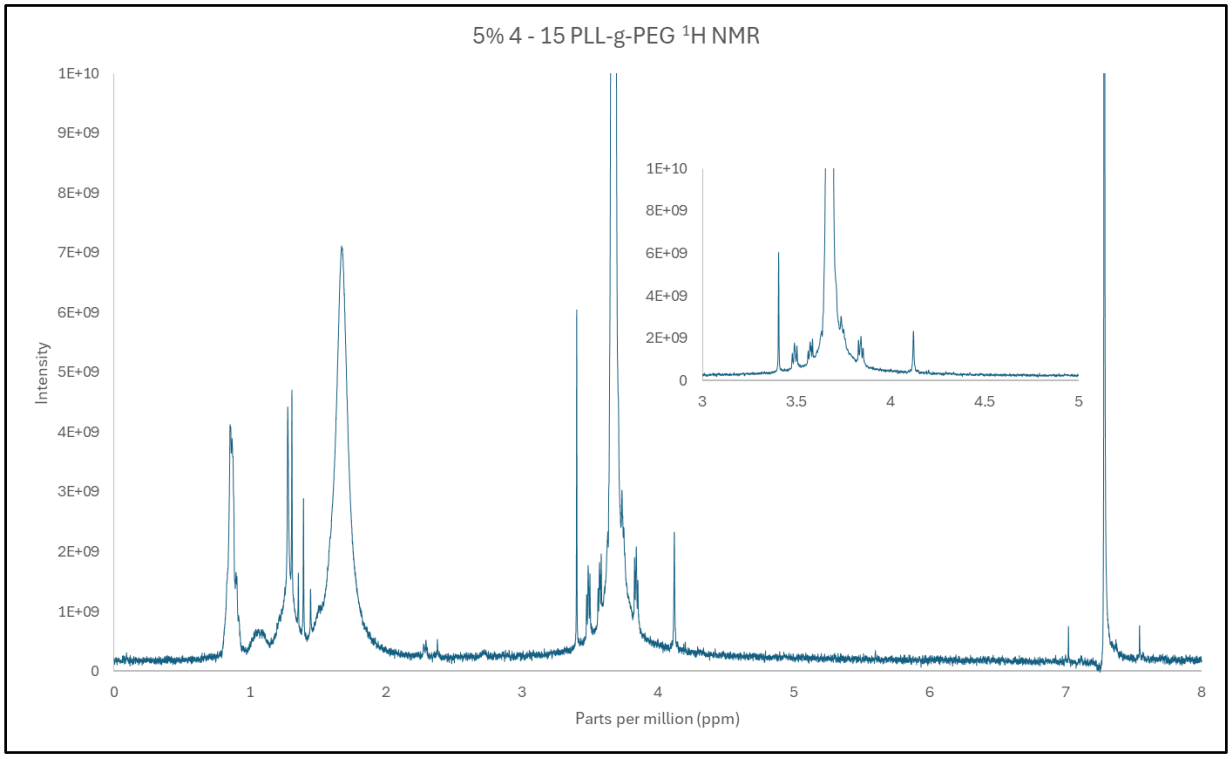

Figure 14. ^{1}H NMR spectrum of 5% PEG grafted 4 – 15 kDa PLL-g-PEG co-polymer in $CDCl_3$

.

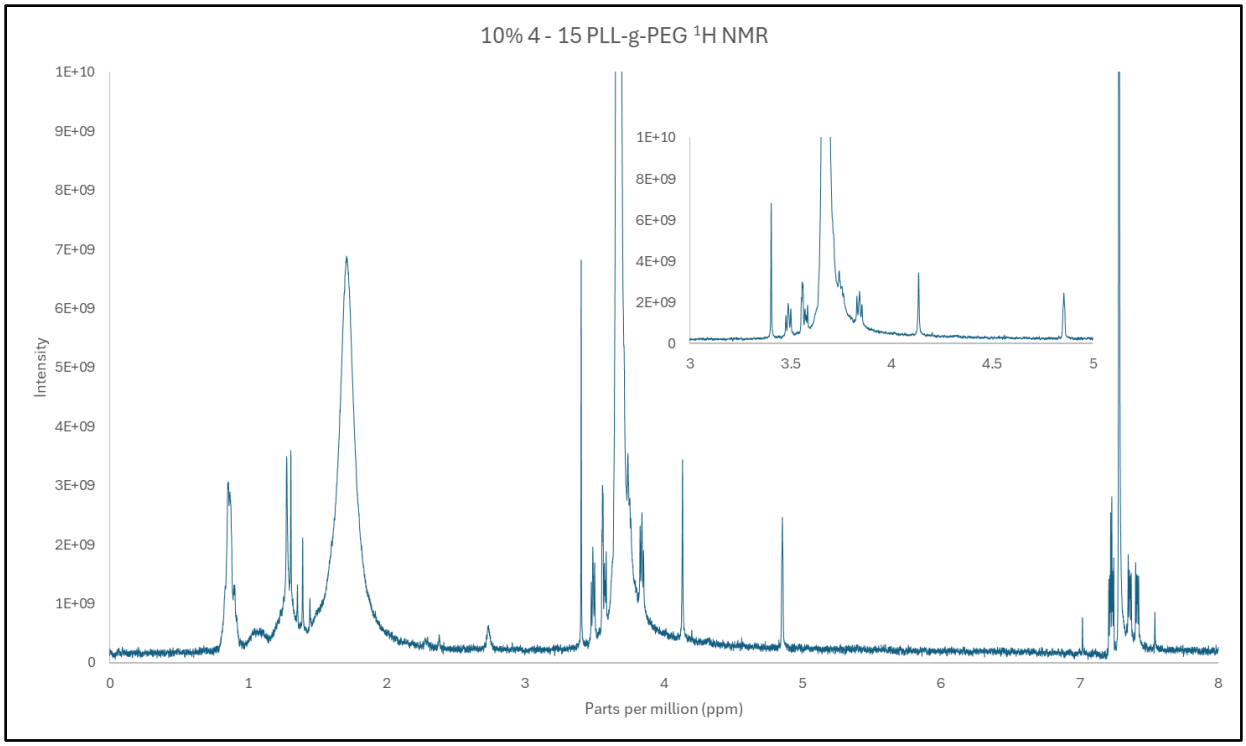

Figure 15. ^{1}H NMR spectrum of 10% PEG grafted 4 – 15 kDa PLL-g-PEG co-polymer in $CDCl_3$

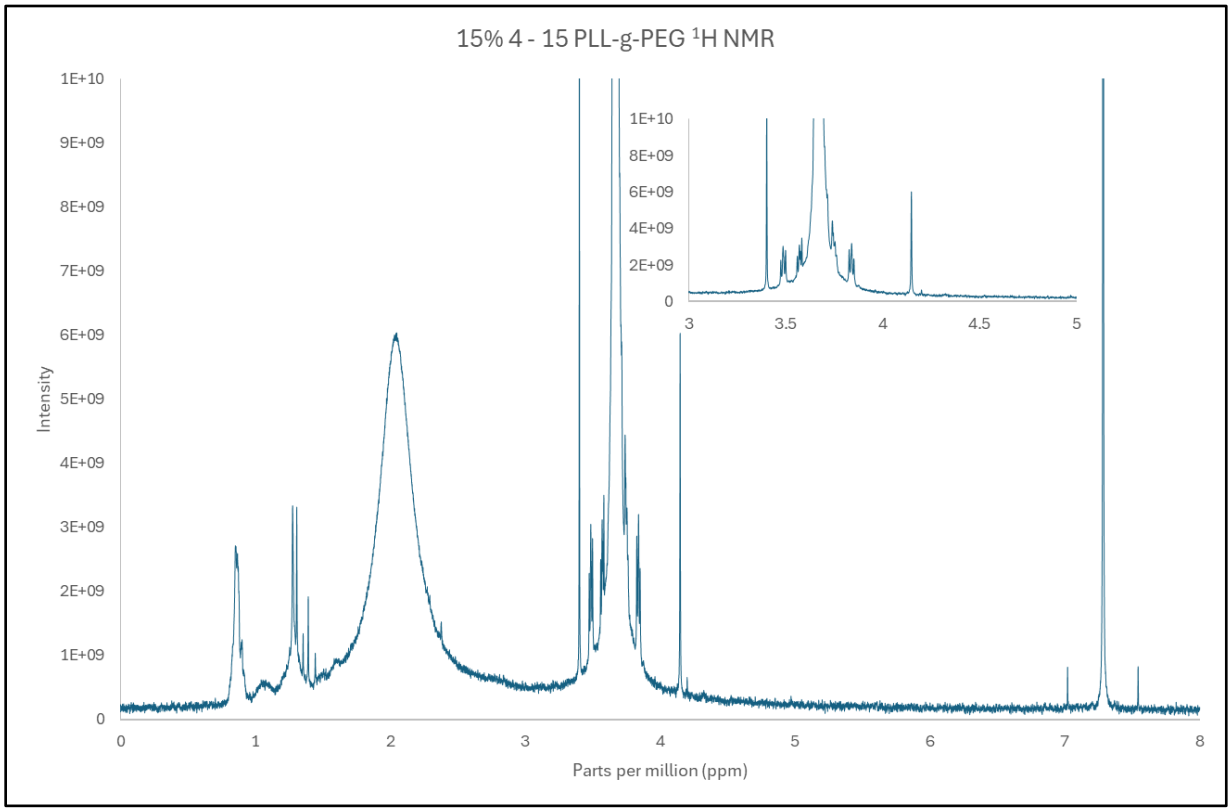

Figure 16. ^{1}H NMR spectrum of 15% PEG grafted 4 – 15 kDa PLL-g-PEG co-polymer in $CDCl_3$

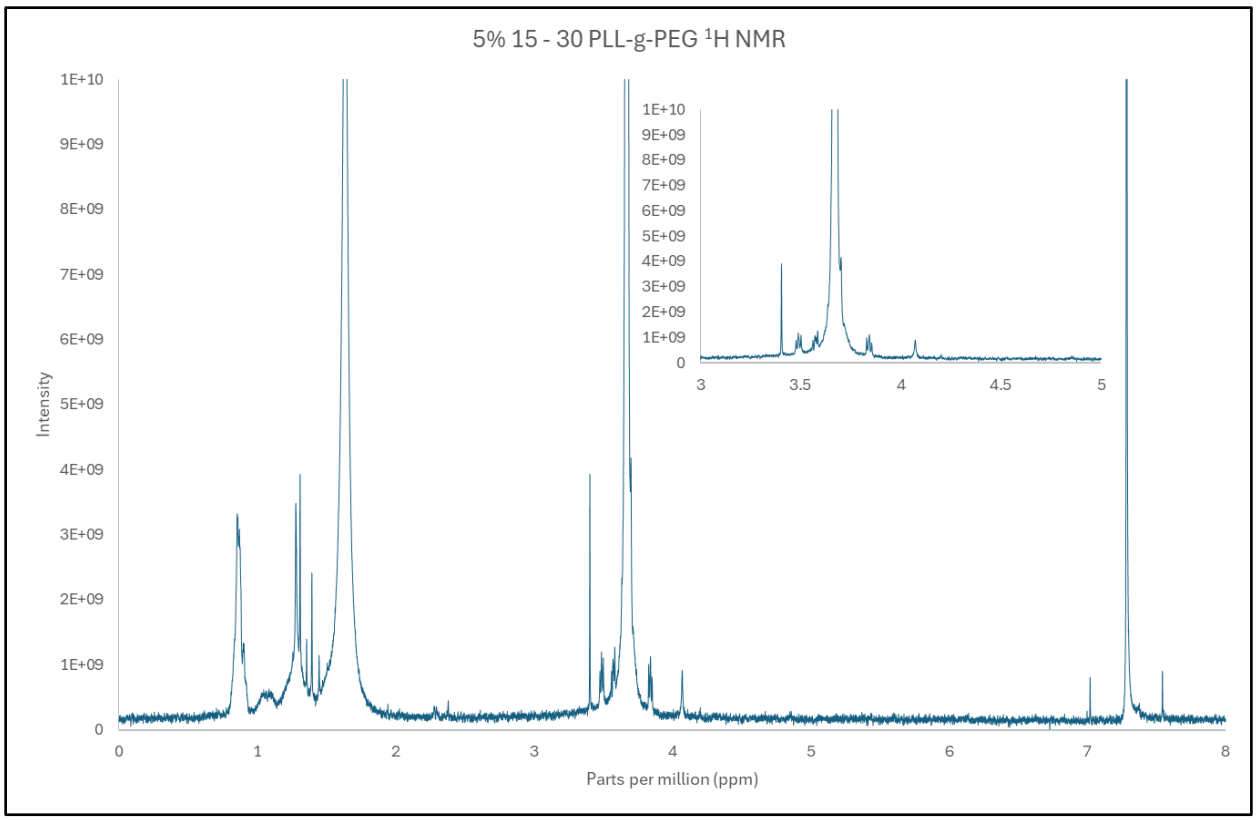

Figure 17. ^{1}H NMR spectrum of 5% PEG grafted 15 – 30 kDa PLL-g-PEG co-polymer in $CDCl_3$

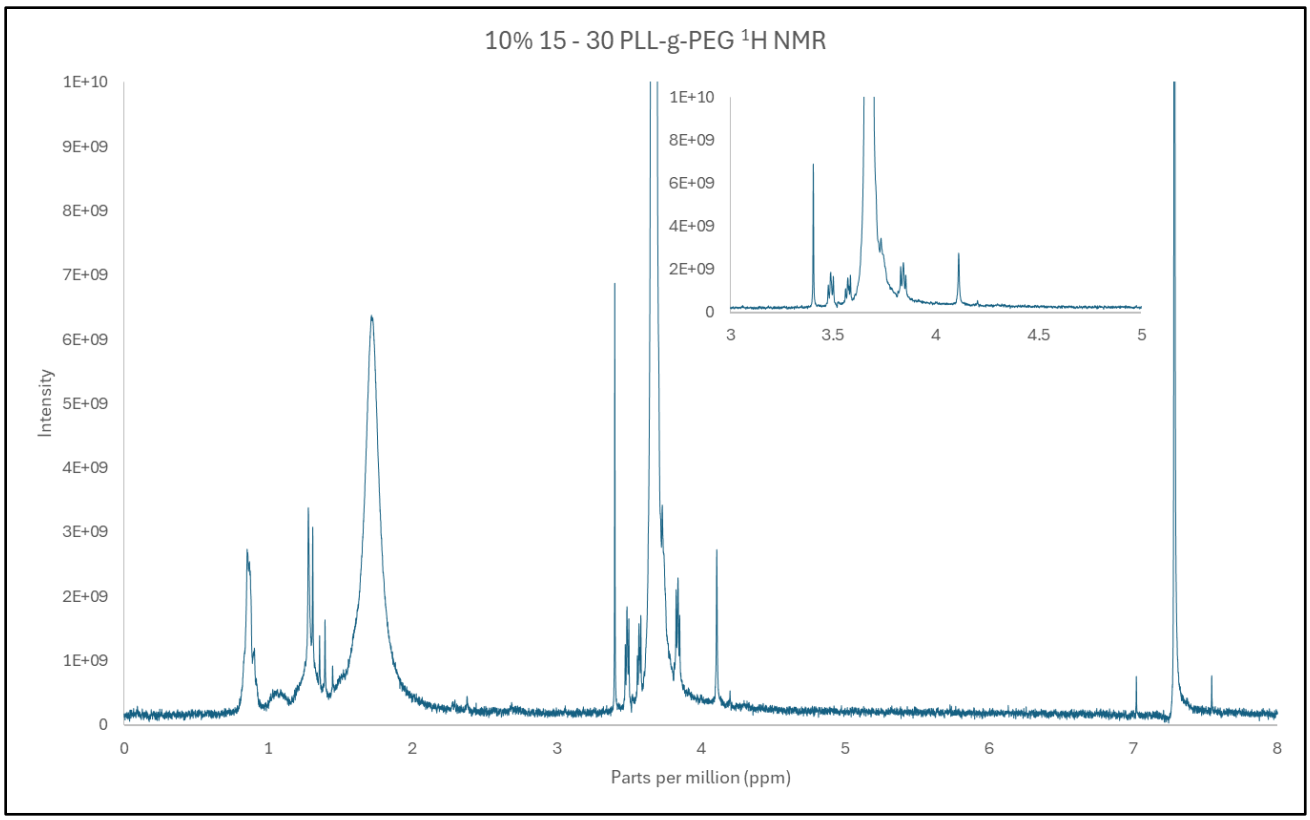

Figure 18. NMR[1]H NMR spectrum of 10% PEG grafted 15 – 30 kDa PLL-g-PEG co-polymer in $CDCl_3$

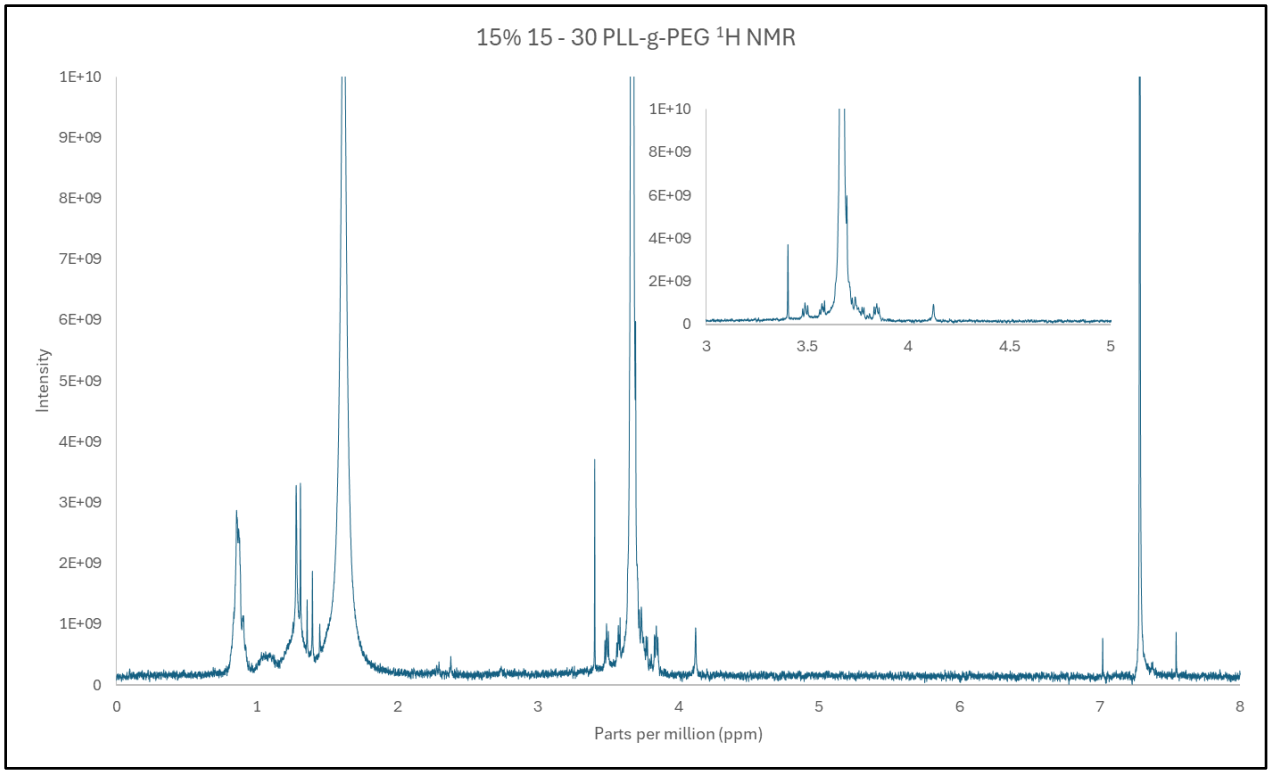

Figure 19. ^{1}H NMR spectrum of 15% PEG grafted 15 – 30 kDa PLL-g-PEG co-polymer in $CDCl_3$

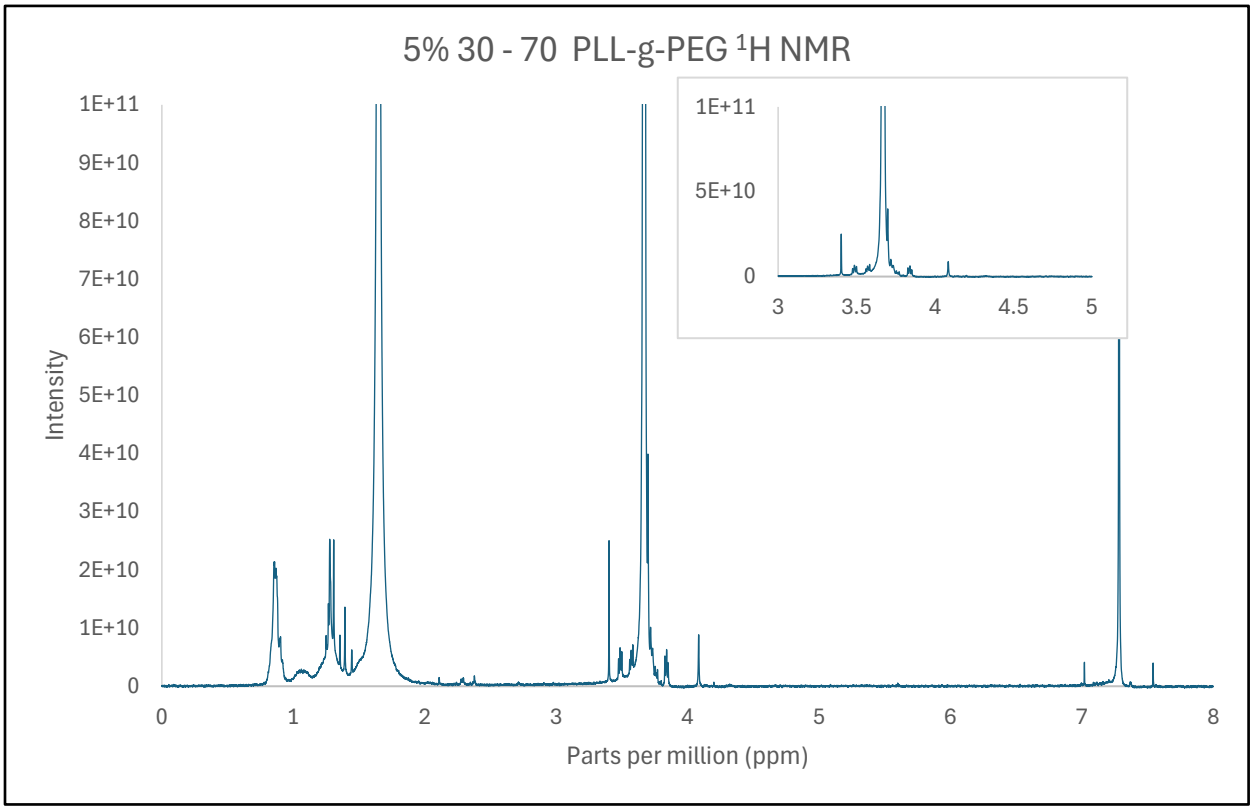

Figure 20. ^{1}H NMR spectrum of 5% PEG grafted 30 – 70 kDa PLL-g-PEG co-polymer in $CDCl_3$

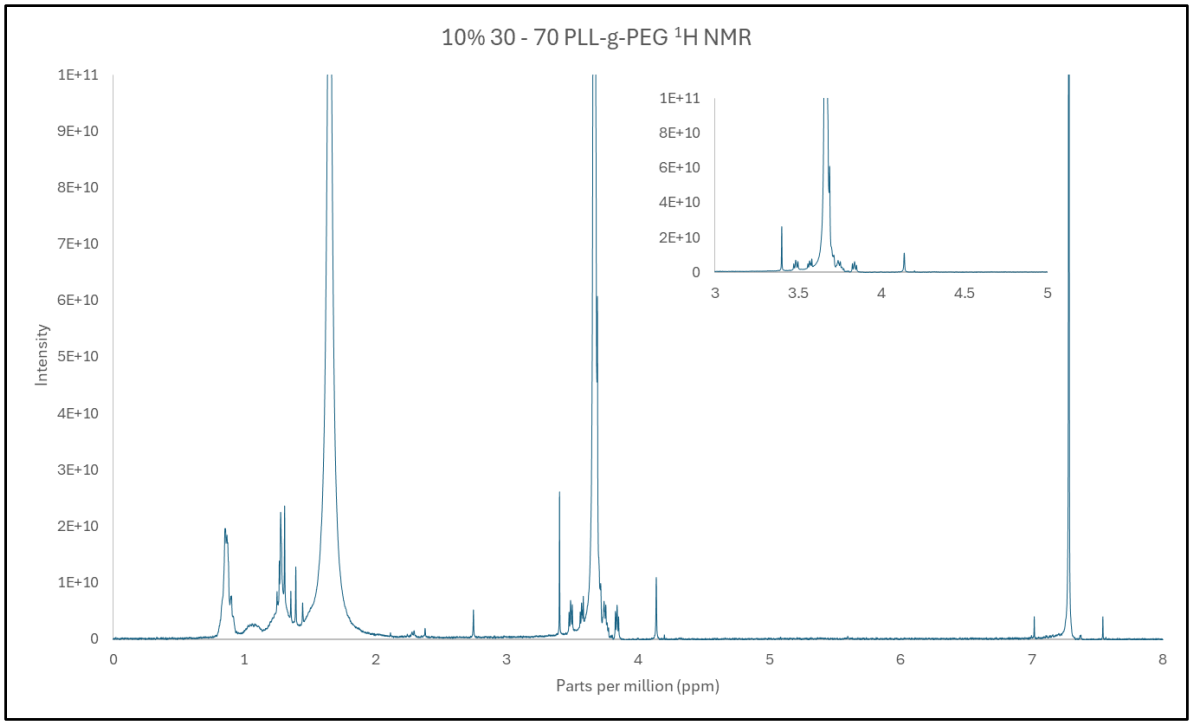

Figure 21. ^{1}H NMR spectrum of 10% PEG grafted 30 – 70 kDa PLL-g-PEG co-polymer in $CDCl_3$

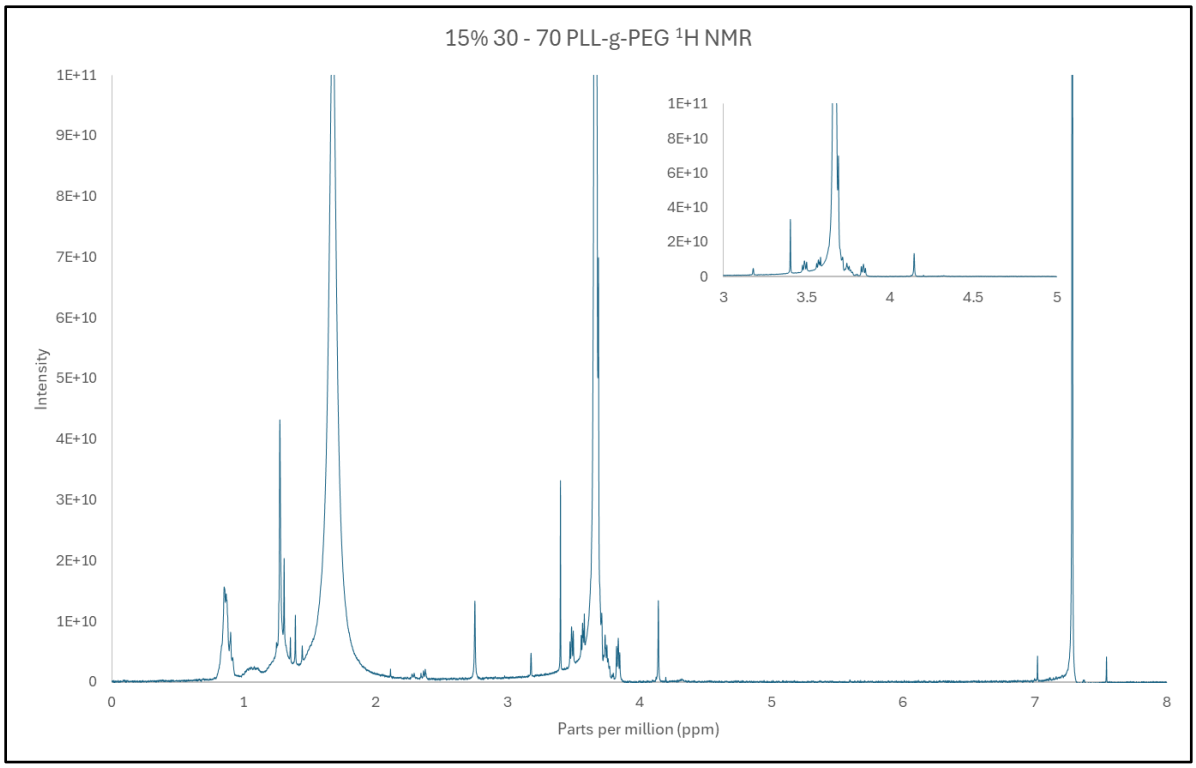

Figure 22. ^{1}H NMR spectrum of 15% PEG grafted 30 – 70 kDa PLL-g-PEG co-polymer in $CDCl_3$

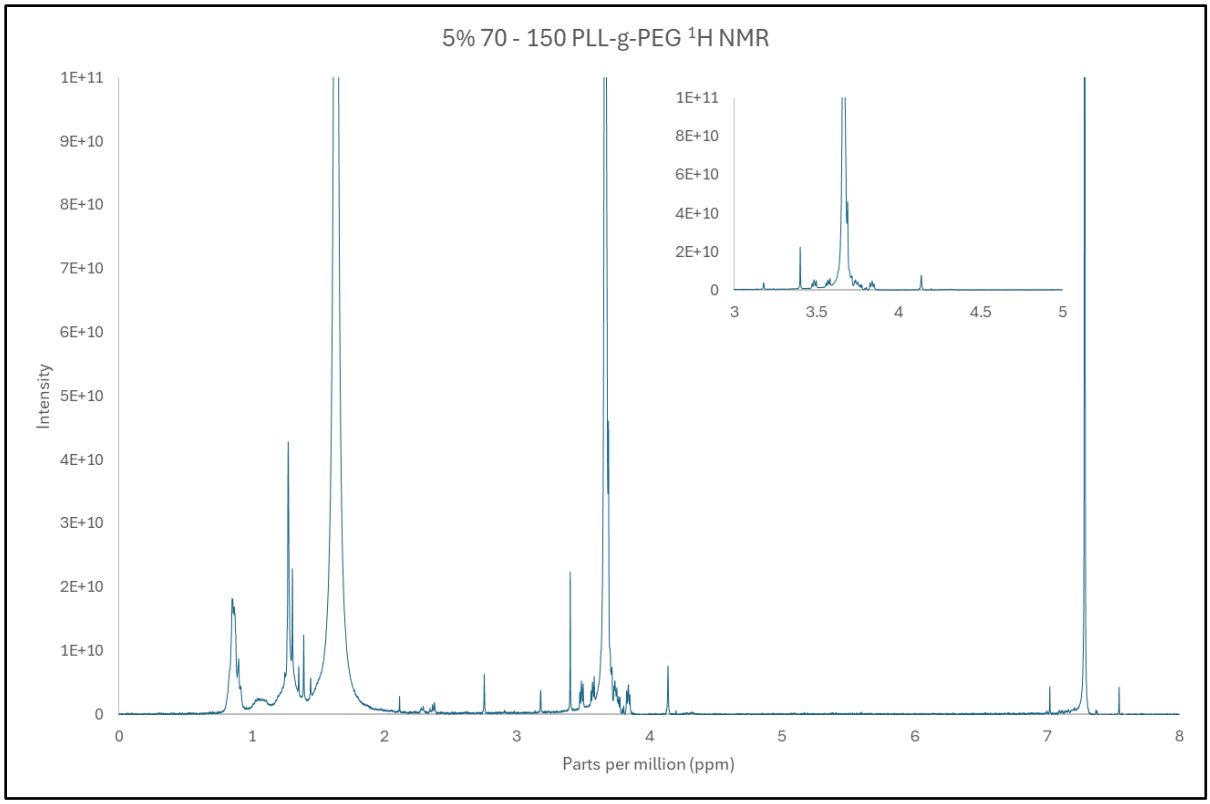

Figure 23. ^{1}H NMR spectrum of 5% PEG grafted 70 – 150 kDa PLL-g-PEG co-polymer in $CDCl_3$

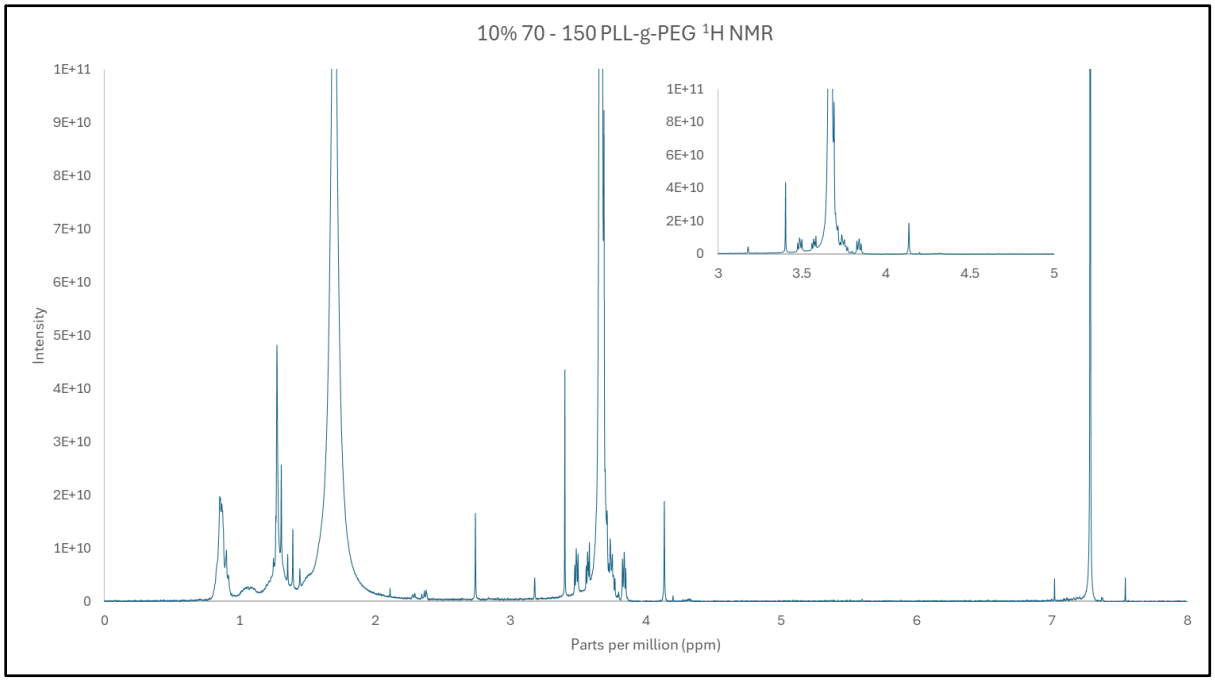

Figure 24. ^{1}H NMR spectrum of 10% PEG grafted 70 – 150 kDa PLL-g-PEG co-polymer in $CDCl_3$

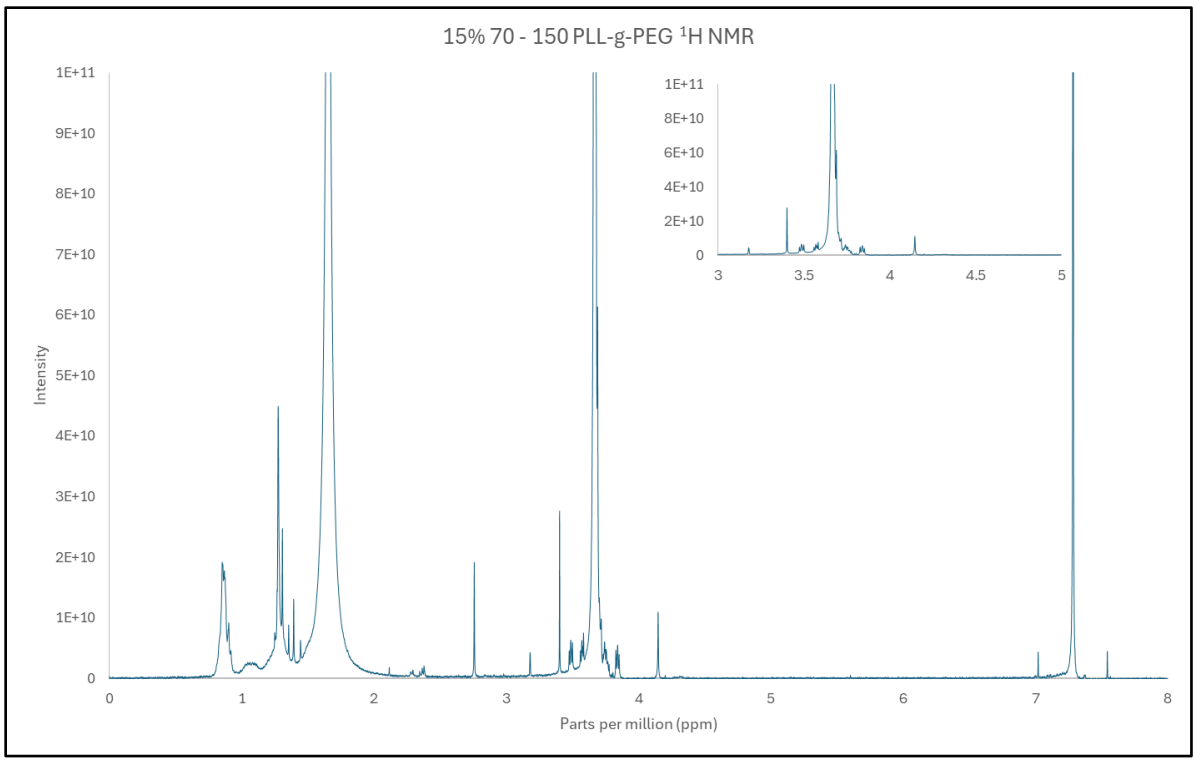

Figure 25. ^{1}H NMR spectrum of 15% PEG grafted 70 – 150 kDa PLL-g-PEG co-polymer in $CDCl_3$

3.5—Physicochemical characterization of NPs

The hydrodynamic diameter of NPs was obtained using DLS to determine the average sizes of BSA NPs. DLS is a technique that primarily measures the Brownian motion of particles in a solution that arises due to bombardment from solvent molecules and relates this motion to the hydrodynamic size of the nanoparticles. Figure 27 summarizes the average hydrodynamic diameter data for all twelve NP samples. The hydrodynamic diameter of the NPs remained fairly consistent, between samples A – K having a hydrodynamic diameter around 20 – 60 nm, despite the increasing molecular weight of PLL or increase in PEGylation % except for Sample L shown in Figure 27 which may be from aggregation of the NPs in solution. The slight differences in NP hydrodynamic sizes can be attributed to possible PEG conformational differences surrounding the particle surface as shown in Figure 26. Grafted PEG chains take on two main conformations: brush or mushroom [24]. depending on factors such as grafting density,

length of the PEG chains, number of repeats, total surface area available, and the solvent present. These confirmational differences may modify the arrangement of water molecules closer to the particle surface in solution which in turn could make slight variations in hydrodynamic diameter. Even though we couldn't directly analyze which confirmation of PEG is present on our NPs, we believe that the different PEG confirmations present in our NP batches may very well explain the sight differences in hydrodynamic diameter we see in Figure 27. Analyzing which configuration of the PEG is present in each NP sample was not an objective of the current project.

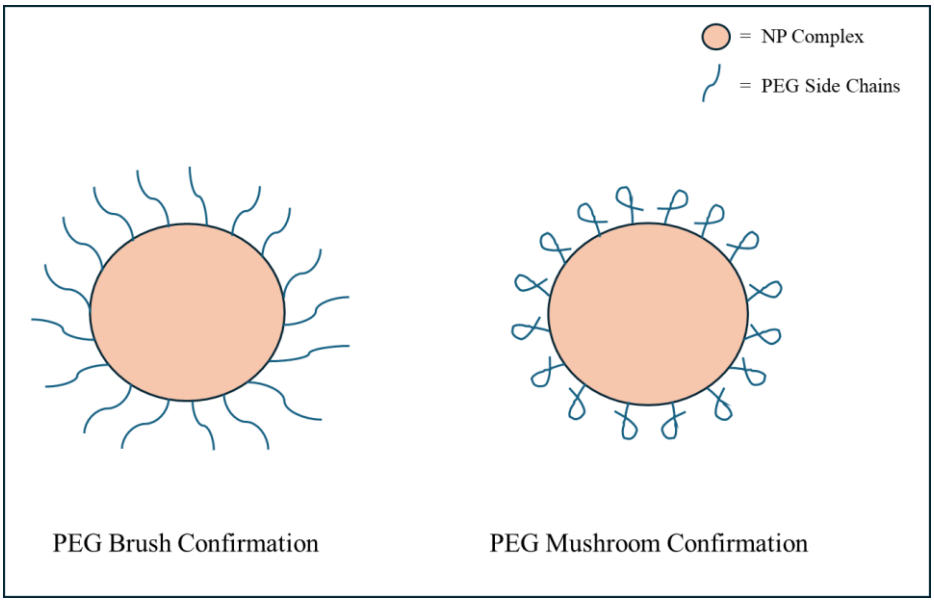

Figure 26. Brush and mushroom conformations of PEG on spherical NPs.

The notable difference seen in Sample L (15% PEGylation onto 70 – 150 kDa PLL NPs) may be a result of aggregation at a higher PEGylation % with longer PLL chains. However, a more accurate measurement of the NP size distribution can be explained from the polydispersity index (PDI) values. PDI is an important parameter that describes the width or spread of the particle size distribution. PDI values can vary from 0 to 1, where the particles with PDIs less than 0.1 implies monodispersed particles and the values more than 0.1 may imply polydispersed particle size distributions. As shown in Table 4, our NPs had PDIs ranging from 0.1-0.5.

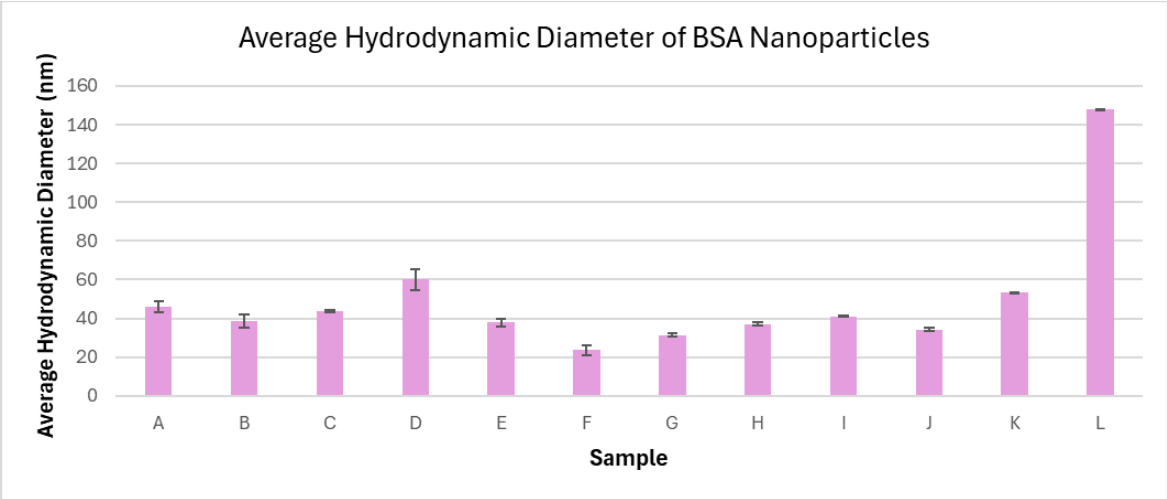

Figure 27. Average hydrodynamic diameter of BSA NPs.

Table 4. PDI values of each BSA NP sample with sample identifier.

Sample Identifier	Description	PDI Values
A	5% 4 – 15 kDa NPs	0.466 ± 0.012
B	10% 4 – 15 kDa NPs	0.475 ± 0.011
C	15% 4 – 15 kDa NPs	0.270 ± 0.013
D	5% 15 – 30 kDa NPs	0.542 ± 0.032
E	10% 15 – 30 kDa NPs	0.302 ± 0.011
F	15% 15 – 30 kDa NPs	0.275 ± 0.025
G	5% 30 – 70 kDa NPs	0.234 ± 0.098
H	10% 30 – 70 kDa NPs	0.207 ± 0.057
I	15% 30 – 70 kDa NPs	0.234 ± 0.075
J	5% 70 – 150 kDa NPs	0.254 ± 0.119
K	10% 70 – 150 kDa NPs	0.177 ± 0.024
L	15% 70 – 150 kDa NPs	0.227 ± 0.005

3.6 Scanning-Transmission Electron Microscopy (STEM) of NPs

Electron microscopy was used to investigate the structure and morphology of NPs. Figure 28 a and b show STEM micrographs of BSA NPs synthesized using 10% PEGylated 4-15 kDa PLL and 10% PEGylated 15-30 kDa PLL, respectively. NP size ranged from approximately 30–40 nm in diameter. While scanning the whole grid, there were a few bigger particles/aggregates observed. These could be due to actual aggregates present or a result of the drop cast drying method that we utilize to make the TEM grids which create layers of NP drying on top of each other. STEM particle sizes agreed well with measurements taken by DLS. NPs were mostly spherical morphology.

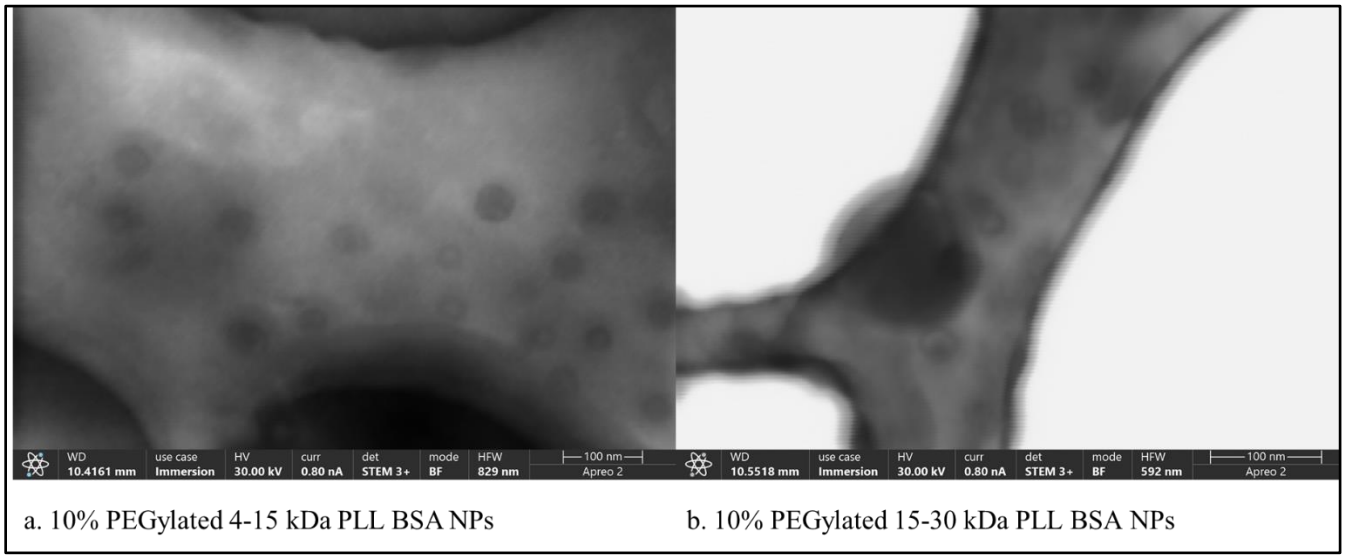

a. 10% PEGylated 4-15 kDa PLL BSA NPs b. 10% PEGylated 15-30 kDa PLL BSA NPs

Figure 28. STEM images of (a) 10% PEGylated 4-15 kDa PLL BSA NPs, (b) 10% PEGylated 15-30 kDa PLL BSA NPs. The scale bar length is 100 nm.

3.7—Evaluation of extent of BSA encapsulation in NPs by SDS-PAGE.

The extent of BSA encapsulation was determined by a gel retardation assay. The experiments were done in two different gels, one containing 5 – 15% PEG grafted, 4 – 15 and 15 – 30 kDa PLL BSA NPs, and a second one containing 5 – 15% PEG grafted, 30 – 70 and 70 – 150 kDa PLL BSA NPs. The results of the gel retardation assays are shown in Figures 29 and 30. Lane 2 of the gels show the protein ladder with molecular weight bands including 250, 130, 100, 70, 55, 35, 25, and 10 kDa. The free BSA control (lane 3) was able to freely migrate down the gel while the migration of NP samples in lanes 4-9 were mostly hindered. NPs are bigger than free proteins and are not able to migrate down the polyacrylamide gel. These NP bands are present right below each well in the stacker region.

However, in all the lanes with NPs we observed streaking (with a gradually decreasing intensity) in the gel, which is a very interesting observation. This could be attributed to a few BSA proteins associated with PLL chains that are loosely bound on the NP surface migrating down the gel or this streaking could also be explained by the staining dye, Coomassie Blue, that has been discovered to bind to a protein's residual lysine groups [25]. The Coomassie dye could bind to the residual lysine groups of the co-polymer, PLL-g-PEG, and produce a streaking pattern that we observe in the gels. Additionally, Figure 5 in the introduction section shows a schematic explanation of the possibility of protein coronas on the surface of NPs and the decrease in streaking intensity that we observe can be correlated to a reduction in the number of residual lysine groups available or a lack of BSA proteins been adsorbed onto a heavily PEGylated surface [13]. Although PLL by itself is not able to migrate down the gel, we believe that a PLL chain that is electrostatically associated with a few BSA proteins could migrate down the gel as a whole and create this type of a streaking appearance as well.

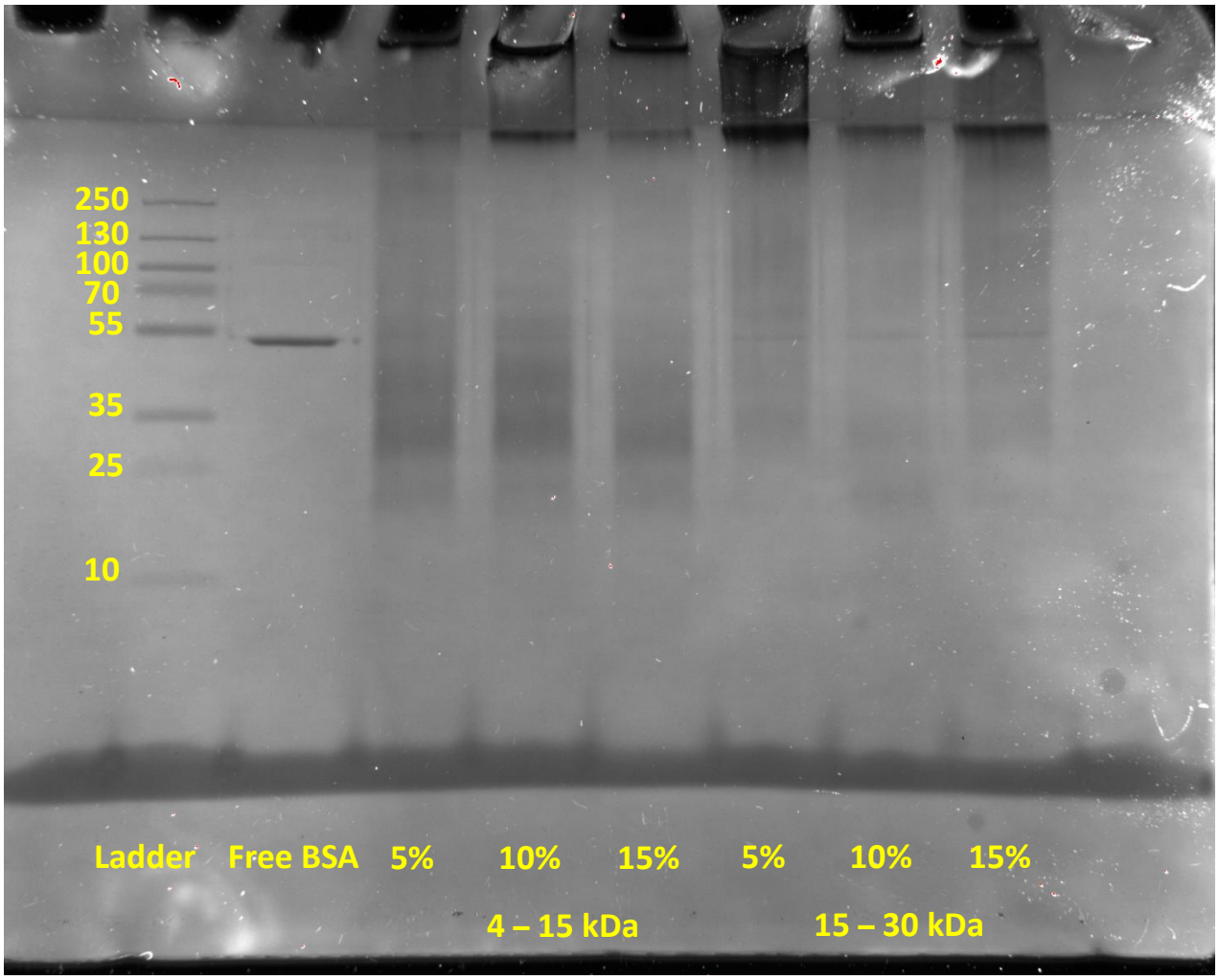

Figure 29. SDS-PAGE (12%) of 5 – 15% 4 – 15 and 5 – 15% 15 – 30 BSA NPs.

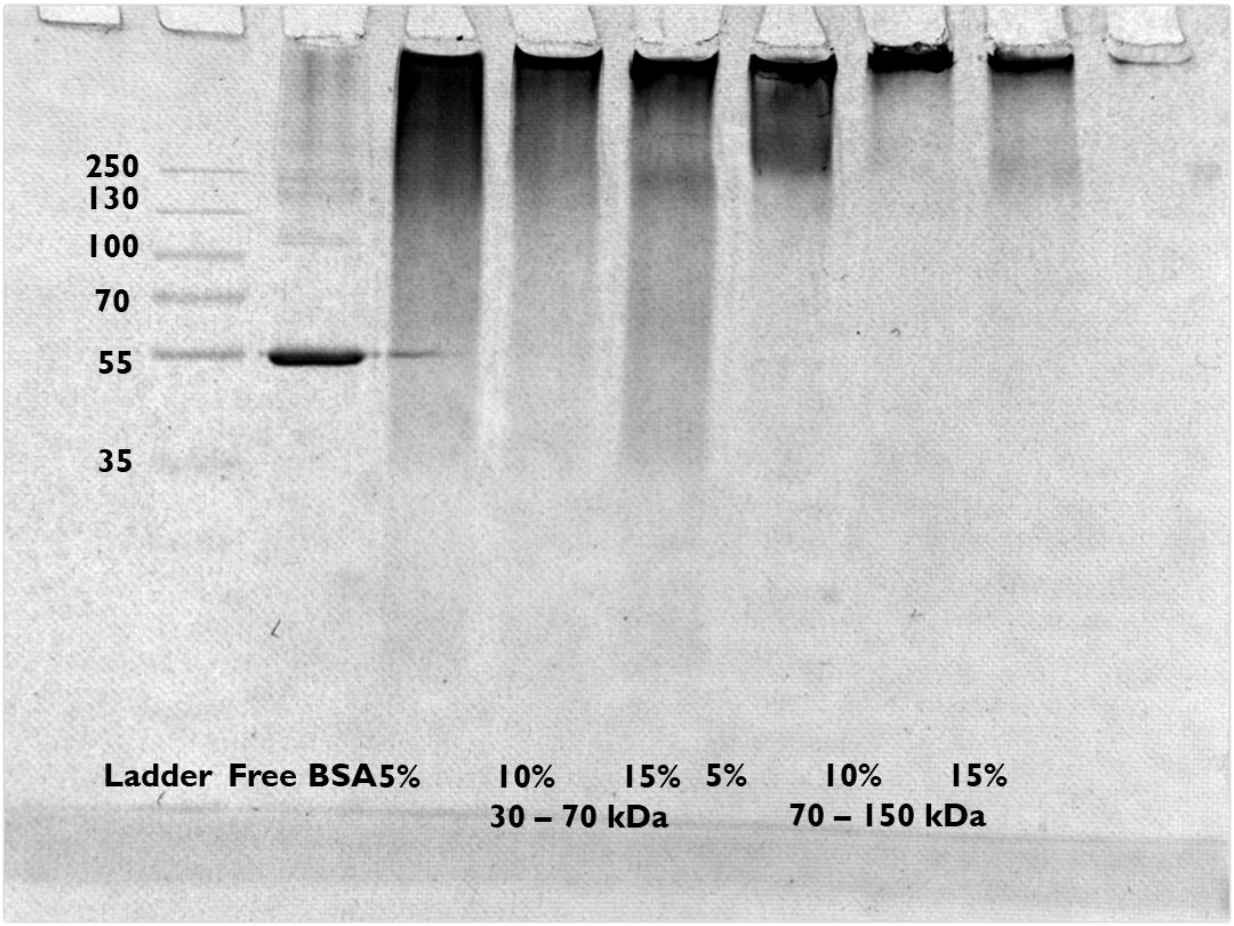

Figure 30. SDS-PAGE (12%) of 5 – 15% 30 – 70 and 5 – 15% 70 – 150 BSA NPs.

3.8—Measurement of Esterolytic Activity of BSA NPs

To evaluate how encapsulation could affect protein function, the hydrolysis of p-nitrophenyl caprylate catalyzed by BSA was measured spectrophotometrically at 412 nm by monitoring the formation of p-nitrophenol. Before the assay, all the NP samples were washed 3 times with PBS using centrifugal protein concentrators to remove any free, non-encapsulated or loosely bound proteins. Figure 31 shows the esterase-like activity of NPs, BSA free NPs, and non-encaspsulaed (free) BSA. Our data indicate that activity of the protein is not negatively affected upon encapsulation nor crosslinking. Interestingly, we observed increased esterase-like activities in BSA encapsulated within the PLL-g-PEG copolymer NPs compared to non-encapsulated BSA. This could be attributed to accumulation of BSA proteins near the

surfaces of these porous, positively charged nanoparticle shells. Although some portion of the activity may be due in part to esterase-like activity from the amine residues in the polymer as shown in BSA free NPs, we still see observe increased esterase-like activities of BSA encapsulated within NPs. Similar particles were prepared with other enzymes have shown increased enzymatic activity (Pope *et al*. 2015; Flynn *et al*. 2019) [26, 27]. Furthermore, our observations were consistent with our previous findings (Flynn *et al*. 2016) and those of others that have produced similar complexes (Yuan *et al*. 2005) [28].

BSA catalyzes the production of p-nitrophenol (PNP) through esterolytic degradation of p-nitrophenyl caprylate. The amount of PNP produced will be directly proportional to the activity of BSA hence to the absorbance measured at 412 nm. Figure 31 shows the absorbance of p-nitrophenol at 412 nm for different NPs compared to that of non-encapsulated free BSA and NPs without any BSA encapsulated. The BSA concentrations of NP samples and the free BSA are kept constant in this experiment to confirm that the differences in esterolytic activity is solely due to encapsulation vs non-encapsulation. However, here we assumed that the encapsulated BSA proteins are equally distributed in our NPs. To accommodate for this assumption, we ran triplicate samples for each NP batch and the activity data shown are the averages.

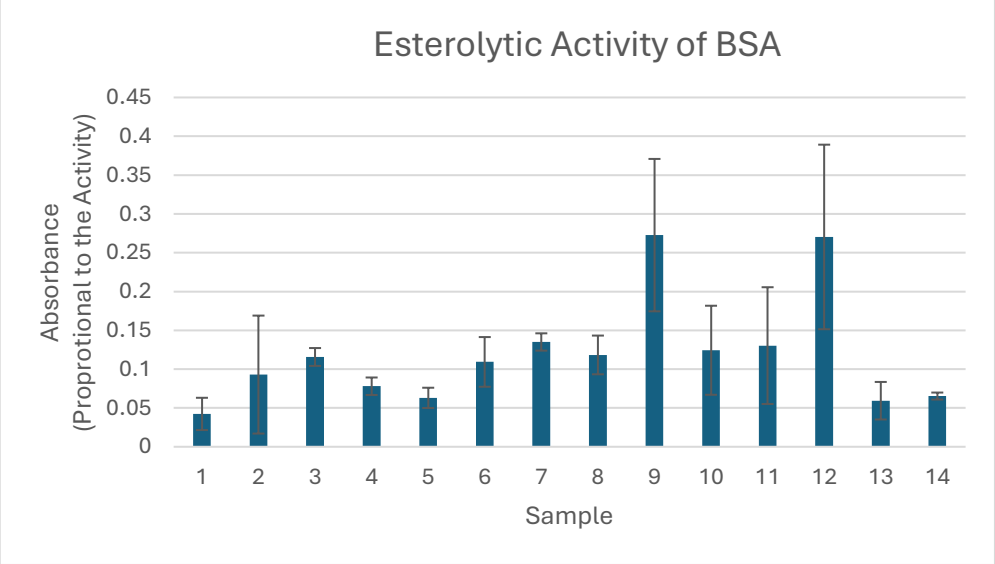

Figure 31. Esterolytic activity of BSA nanoparticles.

Table 5. Esterolytic activity of BSA nanoparticles with sample identifier.

Sample Number	Name
1	BSA Free NPs
2	Free BSA
3	5% 4 – 15 kDa NPs
4	10% 4 – 15 kDa NPs
5	15% 4 – 15 kDa NPs
6	5% 15 – 30 kDa NPs
7	10% 15 – 30 kDa NPs
8	15% 15 – 30 kDa NPs
9	5% 30 – 70 kDa NPs
10	10% 30 – 70 kDa NPs
11	15% 30 – 70 kDa NPs
12	5% 70 – 150 kDa NPs
13	10% 70 – 150 kDa NPs
14	15% 70 – 150 kDa NPs

Our data indicate that activity of the protein is not negatively affected upon encapsulation nor crosslinking. Interestingly, for some NP samples we observed higher esterase-like activities of BSA encapsulated within the PLL-g-PEG copolymer NPs compared to non-encapsulated BSA. Increased catalytic activities upon encapsulation of enzymes have been observed in other studies. Yuan *et al*. reported an increase in catalytic activity of lysozyme encapsulated within α-methoxy-poly(ethylene glycol)–poly(α,β-aspartic acid) block copolymer and crosslinked by glutaraldehyde (Yuan *et al*., 2005) [27]. The authors suggested that the PEG shell around the micelles facilitates substrate accumulation in the micelles, compared to the surrounding, and thus resulted in higher catalytic activity. In our NP

system, the PEGylated PLL network around the protein may similarly facilitate the accumulation of substrate within the NP complex itself.

Overall, our data suggests a general trend of increasing PEGylation resulting in less BSA proteins been adsorbed onto the surfaces of the NP complexes which has affected both our esterolytic activity assay and gel electrophoresis results. The gel electrophoresis figures 29 and 30 have streaking patterns in each lane with NP samples although we note a decreasing intensity in this streaking as the PEGylation of the NP samples increases. This could be a result of less BSA proteins been adsorbed onto the surfaces of these NP complexes or it could be a reduction in the number of residual lysine groups due to the abundance of PEG side chains that react via those lysine -NH_2 groups. We also note that PEGylation percentage affects the esterolytic activity of the BSA in the NP complexes as seen in Samples 9 and 12 in Figure 31. These samples have notably high esterolytic activities compared to other samples with a similar PLL molecular weight yet differing PEGylation percentages. We believe this could be due to less PEGylation on NPs facilitating adsorption of more BSA proteins closer to the NP surface. However, we do not believe that encapsulation of BSA is negatively affected by an increase in PEGylation.

CHAPTER IV

CONCLUSIONS

In the present study, we have successfully synthesized and characterized a library of 12 different PLL-g-PEG co-polymers with varying amounts of PEG grafted onto PLL backbone with 4 different molecular weights; 4 – 15, 15 – 30, 30 – 70, and 70 – 150 kDa. ATR-FTIR and NMR data confirmed the successful synthesis of all the co-polymers. The polymer-protein nanoparticle complexes were formed through electrostatic interactions of the cationic backbone of the PLL-g-PEG copolymers and the negatively charged protein, BSA. The hydrodynamic diameter of the NP batches remained mostly consistent, around 20 – 60 nm, despite the increasing molecular weight of PLL or increase in PEGylation % except for one sample. We speculate that the slight differences in NP hydrodynamic diameters may suggest that the two main PEG conformation, brush and/or mushroom, is possible surrounding the particle surface. STEM particle sizes agreed well with measurements taken by DLS and the NPs were mostly spherical in morphology.

The extent of BSA encapsulation in NPs was partial as evidenced by the streaking and appearance of a free BSA band in some NP preparations as evidenced by SDS-PAGE. Most importantly, we were able prove one of our hypotheses on a possible nanoparticle-protein corona (NP-PC) to be true due to the presence of streaking on our gels. We believe that the streaking with gradually decreasing intensity seen in the gel could be attributed to a few BSA proteins associated with PLL chains that are loosely bound on the NP surface migrating down the gel. The streaking patterns were random and weren't showing any trend as the PEGylation % changed. Therefore, we were not able to draw any conclusions to our other hypothesis where "higher percentages of PEGylation may inhibit BSA being adsorbed onto the surfaces of the nanoparticles due to steric hindrance while lower amounts of PEGylation will allow more BSA proteins to be adsorbed onto the particle surface".

One of the major conclusions of this project is that the activity of the protein is not negatively affected upon encapsulation nor crosslinking as seen in Figure 31. Interestingly, we observed increased esterase-like activities of BSA encapsulated within the PLL-g-PEG copolymer NPs compared to non-encapsulated BSA. The highest esterolytic activity was shown in NPs synthesized using 5% PEG grafted 30 – 70 kDa and 70 – 150 kDa PLL. This could be partially due to the PEGylation % of these complexes. According to Michel *et al*. increased PEGylation can result in these PEG side chains interfering with the adsorption of BSA proteins onto a co-polymer complex [12]. This coincides with our results particularly from the esterolytic activity assay standpoint and this supports our theory that higher amounts of PEGylation will result in less BSA adsorbed onto NP complexes due to dense coverage of PEG side chains restricting BSA protein molecules reaching the surface.

The determination of which PEGylation % will lead to the highest activity of the enzymes encapsulated within PLL-g-PEG co-polymer NPs will enable us to better utilize these nanoparticles as delivery vehicles for protein therapeutics. Additionally, the findings of this project will provide useful insights on how nanoparticle porosity or polymer architecture could be modified for other enzyme related nanoparticle applications.

As we learned in this project the protein corona on NP surfaces could play a significant role in our targeted applications. Therefore, one of the future avenues of research is to explore protein coronas on NP surfaces and the effect of PEGylations % on that including brush and mushroom confirmations. The findings of this project will be applied to other ongoing projects in the lab involving protein activity. This also raises another question which is worth pursuing to know whether higher amounts of PEGylation onto PLL may inhibit the enzymatic activity of encapsulated proteins in general. Another factor to consider is that higher amounts of PEGylation may be necessary because of potential cytotoxic or immunogenic factors depending on the host immune system or cargo being encapsulated. Another

future direction is to investigate lysed NPs to determine how much of the cargo is being encapsulated which will provide a more accurate depiction on how the PEGylation is affecting the cargo uptake.

REFERENCES

1. Baig, N., Kammakakam, I., Falath, W., & Kammakakam, I. (2021). Nanomaterials: A review of synthesis methods, properties, recent progress, and challenges. In *Materials Advances* (Vol. 2, Issue 6, pp. 1821–1871). Royal Society of Chemistry. https://doi.org/10.1039/d0ma00807a
2. Raliya, R., Singh Chadha, T., Haddad, K., & Biswas, P. (2016). Perspective on Nanoparticle Technology for Biomedical Use. *Current pharmaceutical design*, *22*(17), 2481–2490. https://doi.org/10.2174/1381612822666160307151409
3. Mitchell, M. J., Billingsley, M. M., Haley, R. M., Wechsler, M. E., Peppas, N. A., & Langer, R. (2021). Engineering precision nanoparticles for drug delivery. *Nature reviews. Drug discovery*, *20*(2), 101–124. https://doi.org/10.1038/s41573-020-0090-8
4. Chakraborty, A., kumar Singha, D., Chakraborty, M., & Mukherjee, P. (2021). Protein Therapeutics: An Updated Review. In *Citation: Chakraborty A* (Vol. 12, Issue 3). https://www.ijddr.in/
5. Ebrahimi, S. B., & Samanta, D. (2023). Engineering protein-based therapeutics through structural and chemical design. In *Nature Communications* (Vol. 14, Issue 1). Nature Research. https://doi.org/10.1038/s41467-023-38039-x
6. Frokjaer, S. & Otzen, D. E. Protein drug stability: a formulation challenge. *Nat. Rev. Drug Discov.* *4*, 298–306 (2005)
7. Dimitrov D. S. (2012). Therapeutic proteins. *Methods in molecular biology (Clifton, N.J.)*, *899*, 1–26. https://doi.org/10.1007/978-1-61779-921-1_1
8. Hong, S., Choi, D. W., Kim, H. N., Park, C. G., Lee, W., & Park, H. H. (2020). Protein-based nanoparticles as drug delivery systems. In *Pharmaceutics* (Vol. 12, Issue 7, pp. 1–28). MDPI AG. https://doi.org/10.3390/pharmaceutics12070604

9. Kumari, A., Yadav, S. K., & Yadav, S. C. (2010). Biodegradable polymeric nanoparticles based drug delivery systems. In *Colloids and Surfaces B: Biointerfaces* (Vol. 75, Issue 1, pp. 1–18). https://doi.org/10.1016/j.colsurfb.2009.09.001
10. Suk, J. S., Xu, Q., Kim, N., Hanes, J., & Ensign, L. M. (2016). PEGylation as a strategy for improving nanoparticle-based drug and gene delivery. *Advanced drug delivery reviews*, *99*(Pt A), 28–51. https://doi.org/10.1016/j.addr.2015.09.012
11. Rimann, M., Lühmann, T., Textor, M., Guerino, B., Ogier, J., & Hall, H. (2008). Characterization of PLL-g-PEG-DNA nanoparticles for the delivery of therapeutic DNA. *Bioconjugate Chemistry*, *19*(2), 548–557. https://doi.org/10.1021/bc7003439
12. Michel, R., Pasche, S., Textor, M., & Castner, D. G. (2005). Influence of PEG architecture on protein adsorption and conformation. *Langmuir : the ACS journal of surfaces and colloids*, *21*(26), 12327–12332. https://doi.org/10.1021/la051726h
13. Sadeghi, A., PourEskandar, S., Askari, E., & Akbari, M. (2023). Polymeric Nanoparticles and Nanogels: How Do They Interact with Proteins?. *Gels (Basel, Switzerland)*, *9*(8), 632. https://doi.org/10.3390/gels9080632
14. Jahanban-Esfahlan, A., Ostadrahimi, A., Jahanban-Esfahlan, R., Roufegarinejad, L., Tabibiazar, M., & Amarowicz, R. (2019). Recent developments in the detection of bovine serum albumin. In *International Journal of Biological Macromolecules* (Vol. 138, pp. 602–617). Elsevier B.V. https://doi.org/10.1016/j.ijbiomac.2019.07.096
15. Fologea, D., Ledden, B., McNabb, D. S., & Li, J. (2007). Electrical characterization of protein molecules by a solid-state nanopore. Applied physics letters, 91(5), 539011–539013. https://doi.org/10.1063/1.2767206
16. Nguyen, T. X. Q., Chen, S. S., Chang, H. M., Cao, N. D. T., & Singh, R. (2020). Effects of polyethylene glycol and glutaraldehyde cross-linker on TFC-FO membrane performance. *Environmental Technology and Innovation*, *20*. https://doi.org/10.1016/j.eti.2020.101059

17. Salem, M., Mauguen, Y., & Prangé, T. (2010). Revisiting glutaraldehyde cross-linking: The case of the Arg-Lys intermolecular doublet. *Acta Crystallographica Section F: Structural Biology and Crystallization Communications*, *66*(3), 225–228. https://doi.org/10.1107/S1744309109054037

18. Bronze-Uhle, E. S., Costa, B. C., Ximenes, V. F., & Lisboa-Filho, P. N., Synthetic nanoparticles of bovine serum albumin with entrapped salicylic acid. *Nanotechnology, Science and Applications*, 2017, *10*, 11–21.

19. Córdova, J., Ryan, J. D., Boonyaratanakornkit, B. B., & Clark, D. S. (2008). Esterase activity of bovine serum albumin up to 160 °C: A new benchmark for biocatalysis. Enzyme and Microbial Technology, 42(3), 278–283. https://doi.org/10.1016/j.enzmictec.2007.10.007

20. Hikkaduwa Koralege, R.S., Sahoo, K., Flynn, N. *et al.* Erythrocytes internalize nanoparticles functionalized with low molecular weight protamine. *J Nanopart Res* 23**,** (2021) 96-102.

21. Rozenberg, M., & Shoham, G., FTIR spectra of solid poly-l-lysine in the stretching NH mode range. *Biophysical Chemistry*, 2007, *125*(1), 166–171.

22. Khairuddin, Pramono, E., Utomo, S. B., Wulandari, V., Zahrotul, A. W., & Clegg, F., FTIR studies on the effect of concentration of polyethylene glycol on polimerization of Shellac. *Journal of Physics: Conference Series*, 2016, *776*(1), 1-8.

23. Pasek-Allen, J. L., Wilharm, R. K., Bischof, J. C., & Pierre, V. C. (2023). NMR Characterization of Polyethylene Glycol Conjugates for Nanoparticle Functionalization. *ACS omega*, *8*(4), 4331–4336. https://doi.org/10.1021/acsomega.2c07669

24. Cruje, C., & Chithrani, D. B. (2014). Polyethylene Glycol Functionalized Nanoparticles for Improved Cancer Treatment. *Reviews in Nanoscience and Nanotechnology*, *3*(1), 20–30. https://doi.org/10.1166/rnn.2014.1042

25. de Moreno, M. R., Smith, J. F., & Smith, R. V. (1986). Mechanism studies of coomassie blue and silver staining of proteins. *Journal of pharmaceutical sciences*, *75*(9), 907–911. https://doi.org/10.1002/jps.2600750919

26. Pope, C., Uchea, C., Flynn, N., Poindexter, K., Geng, L., Brimijoin, W. S., Hartson, S., Ranjan, A., Ramsey, J. D., & Liu, J. (2015). In vitro characterization of cationic copolymer-complexed recombinant human butyrylcholinesterase. *Biochemical Pharmacology*, *98*(3), 531–539. https://doi.org/10.1016/j.bcp.2015.10.005

27. Flynn, N., Topal, Ö., Hikkaduwa Koralege, R. S., Hartson, S., Ranjan, A., Liu, J., Pope, C., & Ramsey, J. D. (2016). Effect of cationic grafted copolymer structure on the encapsulation of bovine serum albumin. *Materials Science and Engineering C*, *62*, 524–531. https://doi.org/10.1016/j.msec.2016.01.092

28. Yuan, X., Harada, A., Yamasaki, Y., & Kataoka, K. (2005). Stabilization of lysozyme-incorporated polyion complex micelles by the omega-end derivatization of poly(ethylene glycol)-poly(alpha,beta-aspartic acid) block copolymers with hydrophobic groups. *Langmuir : the ACS journal of surfaces and colloids*, *21*(7), 2668–2674. https://doi.org/10.1021/la0488811